

# Lawrence Berkeley National Laboratory

## Recent Work

### Title

THE RADIATION ENVIRONMENT OF HIGH-ENERGY ACCELERATORS

### Permalink

<https://escholarship.org/uc/item/0hr6d57f>

### Authors

Rindi, A.  
Thomas, R.H.

### Publication Date

1973-03-01

c.1

THE RADIATION ENVIRONMENT OF  
HIGH-ENERGY ACCELERATORS

A. Rindi and R. H. Thomas

March 30, 1973

Prepared for the U.S. Atomic Energy Commission  
under Contract W-7405-ENG-48

**For Reference**

Not to be taken from this room



## **DISCLAIMER**

This document was prepared as an account of work sponsored by the United States Government. While this document is believed to contain correct information, neither the United States Government nor any agency thereof, nor the Regents of the University of California, nor any of their employees, makes any warranty, express or implied, or assumes any legal responsibility for the accuracy, completeness, or usefulness of any information, apparatus, product, or process disclosed, or represents that its use would not infringe privately owned rights. Reference herein to any specific commercial product, process, or service by its trade name, trademark, manufacturer, or otherwise, does not necessarily constitute or imply its endorsement, recommendation, or favoring by the United States Government or any agency thereof, or the Regents of the University of California. The views and opinions of authors expressed herein do not necessarily state or reflect those of the United States Government or any agency thereof or the Regents of the University of California.

THE RADIATION ENVIRONMENT OF  
HIGH-ENERGY ACCELERATORS

A. Rindi and R. H. Thomas

Lawrence Berkeley Laboratory  
University of California  
Berkeley, California 94720

30 March 1973

Send proofs to: R. H. Thomas  
Lawrence Berkeley Laboratory  
Bldg. 72, Rm 118  
Berkeley, CA 94720

THE RADIATION ENVIRONMENT OF  
HIGH-ENERGY ACCELERATORS

Contents

1.	Introduction . . . . .	1
2.	The Radiation Environment of Accelerators . . . . .	6
	A. High-Energy Proton Accelerators . . . . .	7
	1. Neutron Spectrometry Techniques . . . . .	9
	a Nuclear Emulsions . . . . .	9
	b Threshold Detectors . . . . .	9
	c Spectrum Determination . . . . .	10
	2. Typical Neutron Spectra Measured at Proton Accelerators . . . . .	12
	B. Electron Accelerators . . . . .	14
	C. Accelerators with Energies > 10 GeV . . . . .	15
3.	Radiation Protection . . . . .	17
	A. The Dose Equivalent . . . . .	17
	B. Dose-Equivalent-Depth Distributions . . . . .	20
	C. Conversion Factors . . . . .	21
4.	Shielding . . . . .	23
	A. Phenomenological Models . . . . .	23
	1. High-Energy Attenuation Length . . . . .	26
	2. Angular Distribution of Secondary Particles . . . . .	27
	3. Accuracy of the Moyer Model . . . . .	30
	B. Monte Carlo Calculations . . . . .	31

5.	Induced Radioactivity . . . . .	33
	A. Radioactivity of Accelerator Components and Other Solids . . . . .	33
	B. Radioactivity of Air . . . . .	36
	C. Radioactivity of Water . . . . .	37
	D. Environmental Impact of Radioactivity . . . . .	38
6.	Conclusions . . . . .	39

## 1. INTRODUCTION

High-energy<sup>1</sup> particle accelerators have been used primarily as physics research instruments. Due, perhaps, to the haste at the beginning for exploiting them, very little thought was given to considering safety measures, and as a result, the radiation environments of these accelerators were initially unknown. The ignorance of accelerator radiation protection in the late forties and early fifties, as described by Rotblat(1), led to underground construction of many of the early synchrocyclotrons(2), avoiding, but inhibiting any fundamental understanding of, radiation problems(3, 4). This solution could not be continued indefinitely. As accelerators grew in physical size, energy, and intensity, and were applied more widely to the problems of medicine, industry, and research, the concern for personnel safety and the pressure of economic considerations made it necessary that accelerator radiation studies be placed on a systematic basis.

Concern for personnel safety was given impetus toward the end of 1948 when it became known that several nuclear physicists in France and the United States, who had been exposed to radiation produced by a cyclotron, had manifested incipient cataract(5). Review of these cases drew attention to the poor status of radiation dosimetry, particularly that of neutrons, at high-energy accelerators. At some cyclotron laboratories immediately there followed extensive effort to improve dosimetric techniques(6, 7): effort further stimulated by the need to reduce radiation levels around accelerators because the successful performance

---

<sup>1</sup>. Any definition of the term "high energy" is necessarily arbitrary. For this review, we may use the term "high-energy accelerator" to mean those accelerators capable of generating  $\pi$ -mesons. This will include most synchrotrons and synchrocyclotrons.

of experimental research often demands radiation intensities one or two orders of magnitude below the maximum level required for personnel safety. The orderly investigation of accelerator-produced radiation required more emphasis on general solutions than was usual in health physics. Over the past decade our knowledge of high-energy radiation environments has made significant advances(8-16) with the operation of several accelerators in the GeV energy region and the design, construction, and operation of several accelerators in the energy region of 10 to 400 GeV.

At high-energy accelerators a large variety of particles may be produced, extending over a wide range of energies, and their measurement presents many novel problems. It was, therefore, necessary to investigate in some detail the production and transmission through shielding of accelerator-produced radiation. Radiation detectors initially designed for nuclear physics research are the natural choice for such investigations. With the understanding provided by such detectors, all the requirements of a radiation protection program may be undertaken(7): possible radiation hazards may be anticipated and their magnitude estimated; protective shielding may be designed and operational procedures selected which permit efficient operation under safe conditions; the response of any radiation detector may be correctly interpreted, and, finally, radiation survey instruments with response approximately proportional to dose equivalent may be designed for use in a limited range of environments.

The lessons learned from the development of techniques of measurement in mixed radiation fields and their interpretation are of general interest because they bear directly on the problem of developing a

general, self-consistent scheme of dosimetry in radiation protection (17-20). Furthermore, experience has shown that the radiation environments of high-energy accelerators are in many respects similar to those produced by lower-energy accelerators or even nuclear reactors: neutrons and photons are the dominant components. So, the techniques of measurement developed for their radiation fields may be applied equally well to both high- and low- energy accelerators.

Experience with accelerator-produced radiation has, until recently, necessarily been limited to a relatively small number of research institutions. However, exposure to accelerator-like radiation environments is no longer only of academic interest. Man's uses of ionizing radiation in research, industry, and medicine have increased dramatically over the past decade. This has been made possible by impressive developments in accelerator design.

A large variety of particle accelerators capable of accelerating a wide range of particles to high energy with high beam intensities is now commercially available. We anticipate a rapid increase in their industrial application to a host of diverse tasks, which has only just begun(21, 22). Burill(23) has documented the increasing uses of accelerators in industry and medicine and shows the number of accelerators in use to be increasing at a rate of roughly 10% per year. Many of the electron accelerators presently being installed are of sufficiently high energy to produce neutrons. Techniques of radiotherapy using fast neutrons,  $\pi$ -mesons, or energetic heavy ions are being extensively investigated(24-26). If widely adopted, considerable numbers of hospital personnel may be occupationally exposed to mixed radiation fields.

There are, in addition, applications of technology that result in exposures to accelerator-like radiation environments. For example, the use of aircraft for mass transportation will expose large numbers of the general population to a radiation environment similar to that produced by high-energy accelerators(27).

There has recently been much speculation and some controversy concerning the possible biological impact on Man of his increasing uses of radiation(28). The effects of low levels on Man are not yet fully understood, but what does seem probable is that radiation effects due to densely ionizing radiations (high LET)<sup>2</sup> will be greater than those due to lightly ionizing radiations (low LET)(29). As we shall see, the radiation environments of many accelerators are particularly rich in high-LET radiation; so, as the uses of accelerators increase, more people may be exposed to high-LET radiations.

In a recent report published by the International Commission on Radiological Protection (ICRP), it is suggested that, in the foreseeable future, high-LET radiations will contribute only a small fraction of the total general exposure(30). Nevertheless, from our present understanding of radiation effects, it is entirely possible that high-LET radiations may have a greater biological impact than this relatively small contribution to exposure might suggest. The possible biological consequences of exposure to high-LET radiation certainly merit continuing study.

---

<sup>2</sup>LET is an abbreviation for Linear Energy Transfer.

In a short review such as this, it is not feasible to attempt an encyclopedic coverage of the entire field of high-energy radiations. Rather, we have attempted to set the development of the subject over the past decade in some perspective by emphasizing those experimental and theoretical advances we believe to be of the greatest importance.

## 2. RADIATION ENVIRONMENT OF ACCELERATORS

Despite the large variety of high-energy particle accelerators, both with respect to beam characteristics and utilization, their external radiation environments are often quite similar, and are dominated by photons and neutrons.

In many branches of health physics it has been customary to quantify radiation fields solely in terms of gross properties such as exposure, absorbed dose and dose equivalent (see section 3 on Radiation Protection). This procedure is inadequate at accelerators. In order properly to perform the tasks required of a health physicist at an accelerator (such as personal dosimetry, the design and construction of radiation-measuring instruments, general radiation and particle beam dosimetry, shielding design or determination of induced activity), it is vital that the detailed composition of the radiation environment be understood in terms of the constituent particles. The study of these environments in terms of the energy spectra of their separate components is still in its early stages; techniques of measurement and data analysis are still being developed, and more extensive measurements are required. Consequently, the limited information that has been published, only describes neutron spectra. But, when supplemented by information from cosmic-ray experiments and neutron transport theory, some general conclusions can be made concerning radiation fields produced by proton accelerators.

Shielding studies have shown that the radiation field reaches an equilibrium condition within a few mean-free paths inside an accelerator shield (see section 4 on Shielding). The shape of the neutron

spectrum observed at a shield/air interface, is very close to that which exists within the shield, but may be perturbed at the low-energy end, due to the scattering and leakage through holes in the shielding.

#### A. High-Energy Proton Accelerators

In the latter part of the fifties, experience at the 184-Inch Synchrocyclotron and Bevatron (Lawrence Berkeley Laboratory) and at the Cosmotron (Brookhaven) estimated the qualitative nature of their radiation environments outside thick shielding (31-34). Although detailed spectra were not obtained, a general rule emerged for proton accelerators, showing that neutrons between 0.1 and 10 MeV contributed more than 50% to the total dose equivalent in the radiation field;  $\gamma$  rays and low-energy neutrons contributed about 10-20%, with the balance made up by neutrons greater than 10 MeV in energy. Patterson et al(35) explained this observation by suggesting that the equilibrium neutron spectrum in the lower atmosphere which is produced by the interaction of the primary galactic cosmic radiation (mainly protons), must be very similar to that generated in the shield of a high-energy proton accelerator. Somewhat later Tardy-Joubert(36, 37) noted that at neutron energies above 50 MeV the neutron spectrum outside the 3-GeV proton synchrotron "Saturne" shield, deduced from an analysis of the prong-number distribution of stars produced in nuclear emulsion, was consistent with the cosmic-ray neutron spectrum measured by Hess et al(38). The relative unimportance of protons is also explained by analogy with the cosmic-ray radiation(36, 39). At energies greater than a few hundred MeV, protons are present in numbers comparable with

neutrons; at lower energies, however, protons are depleted by ionization losses.

By 1965 there was sufficient experience at many high-energy proton accelerators around the world to confirm that the neutron spectra outside accelerator shields and the cosmic-ray spectrum were, in general, quite similar(32-34, 36, 40-42); any attempts to measure proton spectra have not been reported.

There were, however, apparent discrepancies in some data. Table 1 (Ref. 43-45) gives a typical example. The relative composition of dose equivalent measured through thick shielding above an accelerator target is given for a concrete shield and for an earth shield at the CERN proton synchrotron (CPS). The data measured above the concrete shield are very similar to those reported at other accelerators, such as the British 7-GeV proton synchrotron(41), and suggested a neutron spectrum similar to that produced by cosmic rays(35), while the data measured above an earth shield indicated a relatively large contribution to the dose equivalent by high-energy neutrons. Relative data, as in Table 1, are not adequate to determine whether the high fraction of dose equivalent contributed by high-energy particles was due to a deficit of low-energy neutrons or to a surfeit of high-energy neutrons. For this, more specific information on the neutron spectrum would be necessary. In the past ten years more specific information on the shape of the neutron spectra found around accelerators has been obtained by the use of nuclear emulsions and activation detectors(46).

Very little data currently exists in the radiation environments of heavy-ion accelerators but it seems probable that there will be little

qualitative difference from the features exhibited by proton accelerators.

1. Neutron Spectrometry Techniques

a. Nuclear Emulsions. Lehman and Fekula(47) have summarized the neutron spectra determined at the Bevatron from the measurement of recoil protons in thick nuclear emulsions by saying that the general form of the stray neutron spectra (measured between 0.7 and 20 MeV) at eight locations near the Bevatron is a broad peak in the 0.5- to 2-MeV region, followed by a smooth 100-fold drop in value between the peak and 12 MeV. Unfortunately, proton recoil measurements in emulsions are unreliable above about 20 MeV, because track loss corrections become difficult. Nuclear emulsions may be used at higher energies, however, to give some indication of the slope of a smooth neutron spectrum assumed to be of the form  $E^{-n}$ , if the average number of grey prongs per star is determined. This was first done for cosmic rays(48), but the technique has been refined and used outside shielding of accelerators at Berkeley( 49-51). Values of spectral slope,  $n$ , ranging between 1.5 and 2.0 were obtained at the Bevatron and the CPS and are consistent with threshold detector data.

b. Threshold Detectors. The use of threshold detectors is a well understood and universally accepted technique in neutron detection. This technique has found widespread application at most high-energy particle accelerators and has been extensively described in the literature(36, 41, 52-55). Detectors of high sensitivity over the entire energy range normally of interest at accelerators (0.1-100 MeV) are available. For radiation protection purposes, detailed knowledge of

the neutron spectrum in the energy range from thermal up to about 10 keV is rarely required because, as we have seen, intermediate-energy neutrons are usually of little importance. The dose equivalent per unit fluence is independent of neutron energy below 10 keV, and usually a simple measurement of flux density is sufficient. However, detailed spectral information in this energy range may be obtained, if required, by the use of several Bonner spheres of different sizes(56, 57).

c. Spectrum Determination. Measurements with several threshold detectors, whose excitation functions are known, provide information on the energy distribution of the neutron flux density. Specifically, a solution for the neutron spectrum  $\phi(\underline{E})$  is sought from a set of activation equations of the form:

$$\underline{A}_j = \underline{C}_j \int_{\underline{E}_{\min}}^{\underline{E}_{\max}} \sigma_j(\underline{E}) \phi(\underline{E}) d\underline{E} \quad \text{for } j = 1, 2, \dots, m \quad 1.$$

where  $\underline{A}_j$  is the saturation activity of the  $j$ th detector,

$\sigma_j(\underline{E})$  is the cross section for the appropriate reaction at energy  $\underline{E}$ ,

$\underline{C}_j$  is a normalizing constant between activity and flux density, and

$\underline{E}_{\min}$ ,  $\underline{E}_{\max}$  are the minimum and maximum neutron energies in the spectrum.

Equation 1 is a degenerate case of a Fredholm integral equation of the first kind. Formal methods of solution are not applicable when, as is the case with activation detectors, the  $\underline{A}_j$ 's and  $\sigma_j$ 's are known

only as a set of discrete points(58). Early attempts to obtain neutron spectra from activation detector data were frustrated by difficulties such as non-uniqueness or an oscillatory (and even negative) character to the solutions to the Fredholm equations. Some of these problems arise from the mathematical characteristics of the equations to be solved, while others are related to the specific method of solution adopted. Routti(58) has critically reviewed the numerical techniques commonly used for solution of such first-order Fredholm equations, and the interested reader is referred to his paper for a detailed account.

Routti suggests that a suitable method of solution must be able to combine the information contained in the measured data with existing information of the neutron spectrum. Thus, for example, the solution must be non-negative and zero beyond a given maximum energy. In addition, the spectrum of radiation penetrating thick shields constructed of a complex material such as concrete is assumed to be smooth. Some information on intensity or shape may be available from previous measurements. However, care must be taken to ensure that the consequent additional constraints imposed on the spectrum do not prevent it from matching the measured responses or from assuming any physically acceptable shape.

It is important that any method of solution be tested to ensure that it meets all these requirements. This is most conveniently done by computing how the system responds to test spectra. The resolution of the system and the influence of experimental errors or uncertainties in the detector response functions may then be systematically studied.

Routti has applied a generalized least-squares method to solve the activation equations in a computer program LOUHI(59). In his technique, the solution is forced to be non-negative, and prior information on the spectrum can be incorporated. Considerable experience has now been obtained and LOUHI has proved to be extremely reliable and capable of calculating neutron spectra with adequate accuracy for radiation protection purposes.

## 2. Typical Neutron Spectra Measured at Proton Accelerators.

The application of threshold detectors to accelerator radiation environments at several laboratories simultaneously, rapidly expanded our understanding.

Figure 1 shows several typical unnormalized neutron spectra obtained outside thick shields at proton synchrotrons, where  $\underline{E}\phi(\underline{E})$  is plotted as a function of neutron energy [  $\phi(\underline{E})$  is the differential energy spectrum ]. In such a plot,  $1/\underline{E}$  spectrum becomes a horizontal line (Figure 1a). This representation of the Hess cosmic-ray spectrum (Figure 1b) clearly shows the large excess of neutrons in the MeV region (due to evaporation processes) in comparison with a  $1/\underline{E}$  spectrum. At lower energies the spectrum is  $1/\underline{E}$  in character, but there is a noticeable dearth of thermal neutrons.

The neutron spectrum obtained above the concrete shielding around targets at the CPS is shown in Figure 1c. (Compare with Table 1.) The spectrum is seen to be  $1/\underline{E}$  in character from about 1 MeV down to thermal energies. This would be expected from neutron slowing-down theory in a hydrogenous medium, such as concrete. At about 1

MeV the evaporation peak, also evident in the Hess spectrum, is clearly seen, and the spectrum shows a rapid decline at energies above 50 MeV.

Figure 1d shows the neutron spectrum measured above the earth shield of the CPS. (Compare with Table 1.) This spectrum is depleted of neutrons below about 1 MeV, but in other respects is similar to the spectrum shown in Figure 1c. The water content of the earth shield through which the neutrons penetrated was very high (approximately 15% by weight) compared to concrete (few percent by weight,) and so this paucity of low-energy neutrons is to be expected.

The neutron spectrum outside the Bevatron shielding (Figure 1e) is intermediate in character between the two spectra measured at the CPS and suggests that the hydrogen content of the concrete at Berkeley is higher than that at CERN. (To the authors' knowledge this speculation has never been tested.)

Finally, Figure 1f shows the spectrum around a steel-shielded proton beam of the British 7-GeV synchrotron. Compared with the other spectra shown, a large buildup of neutrons below 1 keV is seen, and is attributed to leakage of low-energy neutrons through holes in the shielding(60). It is unlikely, however, that this is the entire explanation because such a buildup is frequently observed outside steel shields. For example, measurements of the neutron spectrum emerging from the main Bevatron magnet identified a very large component near 100 keV(34), while Perry and Shaw(41) observed large increases in radiation levels when steel replaced concrete in shield construction. However, recent theoretical calculations of the neutron spectrum produced in steel by the interaction of 200-GeV protons do not indicate a build-

up(61). Such a discrepancy shows that although we now have a fair understanding of high-energy environments, more needs to be done.

It will be shown later how such neutron spectral data may be used to calculate dose equivalent. Gilbert et al(52) have given the distribution of dose equivalent as a function of energy for several of the neutron spectra shown in Figure 1.

### B. Electron Accelerators

Early measurements at high-energy electron accelerators were principally concerned with the development and transmission of the electromagnetic cascade through the shield(62-66). These studies confirmed that there was good theoretical understanding of these processes(67). Photon spectra at accelerators up to now have not been measured, but a  $\beta$ - $\gamma$  spectrometer and a NaI(Tl) anticoincidence  $\gamma$ -ray spectrometer have been used to measure dose rate for space missions(68, 69). The application of such instruments to accelerator radiation fields may prove illuminating.

Bathow et al(63, 70) measured significant neutron production at the DESY 4-GeV electron synchrotron. De Staebler has shown that at high energies and intensities the radiation environments of electron and proton accelerators will be quite similar outside their shields(71). Increasing attention has been given to the measurement of neutrons in recent years. Thus, for example, measurements outside thick shielding at the Stanford Mark III 1-GeV electron linac showed that neutrons were the dominant component of the radiation field; in addition, a significant flux density of neutrons above 20 MeV was identified(72-74).

Neutrons are a major component of the radiation field(75) in the earth shield, at the 4-GeV electron synchrotron NINA, and are the only significant radiation component surviving at large distances from the SLAC 20-GeV electron linac.<sup>3</sup> Recently Pszona et al (76) have demonstrated the dominating presence of neutrons around the 1-GeV Frascati synchrotron by measurements with ionization chambers.

In making a comparison between the radiation environments of electron and proton accelerators it is interesting to note that close to the primary proton beam, very high photon fluxes have been observed at the 7-GeV synchrotron Nimrod(77) and the CPS(52). The source of these photons has not been established, but has been tentatively attributed to the decay of  $\pi^0$  mesons produced by proton interactions.

### C. Accelerators with Energies > 10 GeV

At high energies (greater than about 10 GeV) the production of energetic muons can be sufficiently great to pose a serious shielding problem at both electron and proton accelerators. Cowan(78) has reported that substantial muon intensities were observed downstream from targets when the BNL 33-GeV AGS first came into operation. Several authors including Keefe(12, 79, 80), Bertel et al(81), Theriot and Awschalom(82), and Kang et al (83) have shown that for the new generation of accelerators above 100 GeV, muons will dominate shielding requirements in regions downstream of beam targets.

At these high energies we need more measurements of neutron spectra outside of various shielding materials in order to study

---

<sup>3</sup>D. Busick, SLAC, private communication.

the influence of shield construction. In particular we need an extension of our knowledge of these spectra above 100 MeV. At these higher energies it may prove to be technically more feasible to detect the equilibrium proton spectrum. Penfold and Stevenson(84) have reported the use of a proton telescope to detect intense sources of radiation inside thick shields along an external proton beam. The application of spark chambers to this problem should prove extremely helpful; Hajnal et al (85) have reported the use of an optical spark chamber to study the secondary-neutron energy spectra emerging from a 40-cm-thick iron shield bombarded by 2.9-GeV protons. A. Rindi(86) and C. B. Lim(87) have described the construction of an instrument utilizing multiwire spark chambers with magnetostrictive readout which may be used for measuring neutron and proton spectra up to energies of about 300 MeV in low-intensity fields.

### 3. RADIATION PROTECTION

#### A. The Dose Equivalent

The numerical scale used in radiation protection is expressed in terms of the parameter dose equivalent whose unit is the rem. Conceptually, dose equivalent is a measure of radiation used in radiation protection, based upon its ability to induce disease (somatic and genetic injury) in humans, who are chronically exposed to low intensities of ionizing radiations(88). (A complete definition of dose equivalent would more adequately define the terms "disease," "chronically exposed," and "low intensities." However, with our present limited understanding of the biological effects of ionizing radiations in humans, such a definition can only be approximated.) Recent discussions in the literature on the methods of evaluating the dose equivalent in high-energy radiation fields, have clarified the concept of dose equivalent. So, we believe it is useful to review this development.

Early observations in radiology and radiobiology suggested that the dominant parameter which largely determined subsequent injury to irradiated tissue was the quantity of energy absorbed per unit mass of tissue. (Absorbed dose is usually measured in units of rads where  $1 \text{ rad} = 100 \text{ ergs g}^{-1}$ .) More sophisticated experiments showed that absorbed dose was not an entirely adequate parameter, and that to better express biological damage, absorbed dose had to be weighted by other parameters, which depended upon the characteristics of the radiation. This problem was empirically solved in radiobiology by expressing exposures to different radiations in terms of absorbed dose of some standard radiation (usually x or  $\gamma$  rays of specified energy). Thus the bio-

logical effects of irradiation by all different types of radiation would be identical to that from  $\chi$  rads of standard radiation where

$$\chi = \sum_{\underline{i}=1}^{\underline{n}} \underline{R}_{\underline{i}} \underline{D}_{\underline{i}} \quad 2.$$

and  $\underline{R}_{\underline{i}}$  is the Relative Biological Effectiveness (RBE) of the  $\underline{i}$ th radiation defined by  $\underline{R}_{\underline{i}} = \underline{D}_{\underline{x}} / \underline{D}_{\underline{i}}$ , and  $\underline{D}_{\underline{x}}$ ,  $\underline{D}_{\underline{i}}$  are, respectively, the absorbed doses of the standard radiation and the  $\underline{i}$ th radiation required to produce the same biological effect.

The quantity defined in Equation 2, that is referred to in the literature as the RBE dose, is clearly an equivalent dose of standard radiation and has the same physical dimensions as those of absorbed dose [as does dose equivalent(89)]. Radiobiologists have measured many RBE's, even for a specific type of radiation, depending upon the biological system, the biological effect considered, the dose rate and distribution, and many other biological and physical factors. One parameter found to have an important influence on the RBE is the average LET, or collision stopping power of the ionizing radiation. [LET still continues to play an important role in the thinking of radiobiologists although recently some have suggested it has only limited value in specifying radiation quality(90-92).]

For radiation protection purposes, the appropriate "RBE's" required would be those for chronic low-level exposures of humans. The biological effects of low-level exposures are not entirely known but probably include carcinogenesis, leukemia induction, life-span shortening and deleterious mutations. There are no data on these bio-

logical effects in humans exposed at sufficiently low doses and dose rates, and furthermore it seems unlikely that data will be directly obtained in the foreseeable future, since such human experiments are not feasible. Nor does it seem likely that epidemiological studies will greatly alleviate this situation, if the risks of somatic injury are of the magnitude estimated by the International Commission on Radiological Protection (ICRP)(93, 94). Any values of RBE currently used in radiation protection are, therefore, extrapolations from epidemiological studies of humans acutely exposed or from animal experiments, and are essentially administrative in character.

The solution adopted by the ICRU/ICRP was to express the "RBE used in radiation protection" as the product of several modifying factors. Provision was made for several such factors including those which take account of LET (the Quality Factor), the nonuniform spatial distribution of absorbed dose, and differences in the absorbed dose rate(95). For external radiation exposure, however, only the Quality Factor ( $\underline{Q}$ ), which accounts for the difference in LET of ionizing radiations at the locations of interest, is defined. When ionizing radiation of more than one LET,  $\underline{L}$ , is present at the point of interest, the dose equivalent at that point may be expressed by a modification of Equation 2 as (96)

$$\underline{H} = \sum_{\underline{i}=1}^{\underline{n}} \underline{Q}_{\underline{i}} \underline{D}_{\underline{i}} \quad 3.$$

In practice, the ionizing particles producing the absorbed dose have a continuous distribution in  $\underline{L}$ , and Equation 3 becomes(97)

$$\underline{H} = \int_0^{\underline{L}_{\max}} \underline{Q}(\underline{L}) \underline{D}(\underline{L}) d\underline{L} \quad 4.$$

where  $\underline{D}(\underline{L})$  is the absorbed dose per unit interval of LET due to particles with LET between  $\underline{L}$  and  $\underline{L} + d\underline{L}$ .  $\underline{L}_{\max}$  is the maximum value of LET at the point of interest. Dose equivalent in high-energy environments is evaluated from a knowledge of the parameters of the radiation environment by calculating the  $\underline{D}(\underline{L})$  distribution as a function of depth and using the relationship between  $\underline{Q}(\underline{L})$  and  $\underline{L}$  defined by the ICRP(98) (Figure 2).

#### B. Dose-Equivalent-Depth Distributions

It is the current practice of regulatory organizations to set maximum permissible limits for the dose equivalent (MPD) in certain so-called "critical organs" such as the gonads, red bone marrow, thyroid, etc. For radiation protection purposes the dose equivalent in these critical organs must be calculated to determine whether those MPD's have been exceeded.

The quantity  $\underline{H}$ , as defined by Equation 4, in principle may be calculated as a function of position in the human body, under any irradiation conditions. In practice, however, such detailed calculations, involving as they do complex details of geometry and nuclear interactions, require extensive computing facilities for their execution. Furthermore, even with the aid of large digital computers, certain simplifications have been necessary to make the calculations tractable.

At present most calculations have been made under limited radiation conditions for uniform, semi-infinite slabs of tissue-like material (e.g., water, polystyrene, "standard-tissue"), but an increasing number of calculations are being made for finite phantoms (parallelepipeds, cylinders, elliptical cylinders). In addition, attention is being given to the effects of nonuniform body compositions(99). In the case of irradiation by neutrons, several summaries of these calculations have been published(100); comparison with experimental measurements indicates good agreement(101).

### C. Conversion Factors

In selecting a single set of particle-flux-density to dose-equivalent rate conversion factors as a function of particle energy, it is conventional to choose those irradiation conditions that maximize the dose equivalent in the body. These generally occur for unilateral irradiation by a normally incident beam of particles. In addition, such conversion factors are derived from the maximum in the calculated dose-equivalent-dose distributions. Figure 3 shows conversion factors for electrons, neutrons, photons, and protons derived in this way by ICRP. In practice it is usually necessary to evaluate dose equivalent due to particles distributed over a range of energies.

The dose-equivalent rate  $\dot{H}$  may be approximated by the equation

$$\dot{H} = \int_{E_{\min}}^{E_{\max}} \phi(E) dE / g(E), \quad 5.$$

where  $g(E)$  is the appropriate conversion factor for particles of energy  $E$ , and  $E_{\min}$ ,  $E_{\max}$  are the appropriate energy limits.

Because the conversion factors  $g(E)$  are derived from irradiation conditions which maximize the dose at each energy, the use of Equation 5 may overestimate the dose equivalent due to a continuous particle spectrum. Equation 5 expresses the sum of the maxima of the dose-equivalent depth curves at each energy rather than the maximum of the sum of the dose-equivalent distributions from each component of the spectrum(102).

For irradiation by particles extending over a wide energy range, Shaw et al (17) have suggested that the dose equivalent should be obtained by calculating the dose equivalent distribution in the body due to the entire spectrum. The maximum dose equivalent in the body (or the dose equivalent in the internal organs) may then be evaluated. They have reported such calculations for some typical accelerator neutron spectra (Figure 1) and showed that the use of Equation 5 with these spectra was accurate enough for practical purposes. This may be seen from Table 2, which compares effective conversion factors averaged over the entire energy range. In column 1 is given approximate values obtained using Equation 5 [reported by Gilbert et al (52)]; Column 2 gives more precise values reported by Shaw et al (17). There is essential agreement between these two sets of values.

#### 4. SHIELDING

As recently as 1960, Jaeger described the design of high-energy radiation shielding as "more an art than a science" (103). During the period 1960-1970, several experiments at high-energy electron and proton accelerators as well as theoretical studies of the propagation of radiations through shielding have radically changed the state of the art. A critical review of many of these experiments has recently been given by Patterson and Thomas(3, 4), and Ranft(104) has compared experimental data with Monte Carlo calculations.

The immediate aims of the early experiments were to obtain a qualitative understanding of the transmission of accelerator-produced radiation, to express this understanding in some physically plausible, but empirical manner, and, finally, to make this empirical formulation quantitative. As our understanding of radiation transport increased, experiments became more sophisticated in an attempt to understand the development of electromagnetic and hadronic cascades in matter. Now, as theoretical techniques become increasingly reliable, experiments are designed with a view of testing (and improving) theoretical models of transport phenomena.

##### A. Phenomenological Models

Consider an effective point source produced by protons interacting in a thick target (Figure 4). The radiation level on the outside surface of a shield may be written, by analogy with the corresponding photon shielding problem as

$$\underline{H} = \frac{1}{\underline{r}^2} \int \underline{F}(\underline{T}) \underline{B}(\underline{T}) \exp\left(\frac{-\underline{d}(\theta)}{\lambda(\underline{T})}\right) \cdot \frac{d^2 \underline{n}(\underline{T}, \theta)}{d\underline{T} d\Omega} d\underline{T}, \quad 6.$$

where  $\underline{r}$  is the distance from the source,  
 $\underline{T}$  is the neutron energy,  
 $\underline{F}$  is a factor which converts fluence to dose equivalent,  
 $\underline{d}$  is the shield thickness,  
 $\lambda$  is the effective removal mean-free path,  
 $\underline{B}$  is a buildup factor, and  
 $\frac{d^2 \underline{n}}{d\underline{T} d\Omega}$  is the yield of neutrons per unit solid angle between  $\underline{T}$   
and  $\underline{T} + d\underline{T}$  at angle  $\theta$ . (See Figure 4.)

De Staebler(8) wrote Equation 6 as:

$$\underline{H} = \frac{1}{\underline{r}^2} \sum_{\underline{i}} \underline{B}_{\underline{i}} \underline{F}_{\underline{i}} \exp\left(\frac{-\underline{d}}{\lambda_{\underline{i}}}\right) \cdot \left(\frac{d\underline{n}}{d\Omega}\right)_{\underline{i}} \quad 7.$$

where the subscript  $\underline{i}$  denotes a range of neutron energies for which  $B$ ,  $F$ , and  $\lambda$  are fairly constant and the definition of  $(dn/d\Omega)$  is obvious.

Moyer(105, 106) made an extremely important contribution when he recognized that Equation 7 may be approximated by a single energy group because the nature of the radiation field outside the shield of a high-energy proton accelerator will be determined by neutrons with energy greater than about 150 MeV. Neutron attenuation lengths above 150 MeV are roughly independent of energy, but diminish rapidly with energy below about 100 MeV. Consequently, the greater yields of low-energy as compared to high-energy neutrons, at the primary interaction, will be more than compensated for by the greater attenuating action of the shield for these

neutrons. Deep in the shield, high-energy ( $E > 150$  MeV) neutrons regenerate the cascade but are present in relatively small numbers. At a shield interface the radiation field observed consists of these "propagators," born close to the primary radiation source, accompanied by many particles of much lower energy born near the interface. Equation 7 therefore becomes

$$\underline{H} \propto \frac{N g(\theta)}{r^2} \cdot \exp(-d/\lambda) \quad 8.$$

where  $\underline{N}$  is the proton intensity incident on the target,  
 $\theta$  is the angle subtended to the beam direction,  
 $g(\theta)$  is the angular distribution of high energy particles at the source,  
 $\underline{d}$  is the shield thickness, and  
 $\lambda$  is the effective attenuation length of high-energy neutrons.

The total neutron flux density (and consequently the dose-equivalent rate) will be proportional to the high-energy neutron flux density. Because the low-energy components are produced by interaction of the high-energy propagators, their intensity decreases through the shield in an exponential manner with effectively the same attenuation length for all directions through the shield.

Moyer(105, 106) generated appropriate parameters to be used in Equation 8 in calculating shielding for the Bevatron. Smith(54) has described the excellent agreement between measured radiation levels outside the Bevatron shield and those predicted by Moyer.

Many shielding experiments have subsequently confirmed Moyer's basic assumptions. For example, Smith et al (55) used threshold detectors to measure the spatial variation of flux density produced in concrete bombarded by 6-GeV protons. Figure 5 shows the relative flux density distribution, measured by the  $^{27}\text{Al} \rightarrow ^{24}\text{Na}$  reaction (threshold 6 MeV) along paths drawn at several angles to the incident beam direction. The transmission curves are seen to be exponential and essentially parallel, within the limits of experimental accuracy. Similar results were obtained with detectors utilizing the  $^{12}\text{C} \rightarrow ^{11}\text{C}$  reaction (threshold 20 MeV). In addition, Smith et al demonstrated the existence of an equilibrium spectrum by calculating the ratio of the response of the carbon and aluminum activation detectors. Figure 6 shows that this ratio becomes constant both in the beam direction and transverse to it. Equilibrium is evidently much more rapidly attained in the transverse direction than in the beam direction.

In the past five years effort has been devoted to obtaining optimum values of  $\lambda$  and  $g(\theta)$  for use in Equation 8.

#### 1. High-Energy Attenuation Length

It is readily seen that the results of calculations using the Moyer model are most sensitive to the value of attenuation length used. At high energies, particle attenuation is essentially determined by inelastic interactions and so we might expect the appropriate value of  $\lambda$  to be given by

$$\lambda = \frac{1}{N \sigma_{\text{in}}} \quad 9.$$

where  $\underline{N}$  is the number of atoms/cm<sup>3</sup> and  $\sigma_{\underline{in}}$  is the inelastic cross section.

Measurements of nucleon-nucleus inelastic cross sections as a function of mass number are quite well represented by the formula

$$\sigma_{\underline{in}} = 43.1 \underline{A}^{0.70} \text{ mb,} \quad \text{for } \underline{A} \geq 3, \underline{E} \geq 150 \text{ MeV,} \quad 10.$$

irrespective of whether the incident particle is a proton or neutron(107, 108). Substitution into Equation 9 gives

$$\rho \lambda = 38.5 \underline{A}^{0.30} \text{ g cm}^{-2}. \quad 11.$$

Over the past fifteen years many shielding experiments have been performed(3, 4), but accurate data are limited. The earlier experiments, in particular, were subject to many sources of error, especially with regard to an accurate knowledge of the density of the shielding material. Furthermore, in much of the earlier literature there are conflicting interpretations of the term "attenuation length"(3, 4). Of the later experiments, that reported by Gilbert et al (52) at the CPS, which analyzed the experimental data in terms of the Moyer model, obtained a value of  $\lambda = 117 \pm 2 \text{ g/cm}^2$  in earth, close to that predicted by Equation 11. Use of attenuation lengths calculated from Equation 11 is certainly consistent with the available experimental determination of attenuation length.

## 2. Angular Distribution of Secondary Particles

The exact nature of the angular distribution function  $g(\theta)$  that should be used in Equation 8 is not immediately obvious. One approach is to deduce angular distribution from measurements of particle flux

density within the shield around the radiation source. Using such an approach, Gilbert et al (52) found that an angular distribution of the form

$$g(\theta) = \underline{a} \exp(-\underline{b}\theta) \quad 60^\circ \leq \theta \leq 120^\circ \quad 12.$$

well represented the flux density data measured in the earth shield of the CPS. In these measurements a thin Be-Al target was bombarded by 14.6 or 26.4 GeV/c protons. In their experiment the parameter  $\underline{b}$  did not seem to be strongly dependent upon primary proton energy. Values of  $\underline{b}$  in the range 2.1-2.4 radian<sup>-1</sup> were reported by Gilbert et al consistent with values of  $\underline{b}$  around 2.5 reported by Stevenson et al (109), using a similar technique, for a primary proton energy of 7 GeV.

The angular distribution of secondary hadrons determined from measurements around fairly thin targets is of more fundamental interest. Such data are needed to test the validity of Monte Carlo and other transport model calculations, which are used increasingly to estimate the magnitude of a variety of radiation phenomena such as radiation damage, induced radioactivity, and radiation intensity. Measurements of momentum-integrated secondary-particle yields around internal targets are difficult because of poorly defined source geometry(52, 110). Recently some careful measurements of the angular dependence of hadron yields from various target materials bombarded by 3-GeV(111), 7-GeV and 23-GeV(112) protons have been reported. Levine et al(112) conclude from their measurements that the shape of the angular distribution measured with any particular detector is independent of primary proton energy and, within the range  $60^\circ \leq \theta \leq 120^\circ$ , is consistent with the form suggested

by Gilbert et al (52) (Equation 12). Table 3 summarizes values of the parameter  $\underline{b}$  obtained at 7 GeV, from which it may be concluded that  $\underline{b}$  is strongly dependent upon the energy threshold of the radiation detector. Comparison with the 3-GeV data of Awschalom and Schimmerling(111) indicates no strong dependence of  $\underline{b}$  upon primary proton energy. Figure 7 shows the data of Table 3. (A range for threshold energy is indicated because different hadrons may produce the radioactive species observed.)

In using the Moyer model to calculate transverse shielding for proton accelerators, the appropriate angular distribution  $\underline{g}(\theta)$  is assumed to be that of particles with energies greater than about 150 MeV(105). Extrapolation of the data of Figure 7 gives a value of  $\underline{b}$  of  $2.3 \pm 0.3$  at 150 MeV. This value is in surprisingly (and perhaps fortuitously) good agreement with the values of  $\underline{b}$  in the range 2.1-2.5 extrapolated from measurements deep in the shield.

The absolute yield of secondary hadrons depends both upon target material and primary proton energy. At large angles the yields appear to be dominated by contributions from the intranuclear cascade and are not inconsistent with a variation proportional to  $A^{1/3}$ (112). If the yield  $\underline{y}$ , is expressed in the form

$$\underline{y} = \text{constant} \cdot \underline{E}^{\underline{n}} \cdot \underline{g}(\theta) \quad 13.$$

$\underline{n}$  lies in the range 0-0.5, depending upon the detector used, over the angular range  $30^\circ \leq \theta \leq 80^\circ$ .

Comparison of the experimental with the integrated momentum spectra of secondary particles predicted by a modification of the semi-empirical Trilling production formula(113, 114) indicates good absolute

agreement at angles less than  $30^\circ$ . At larger angles there is a divergence between the experimental data and theoretical predictions for two reasons: Firstly, this Trilling formula does not correctly describe the production of particles with high transverse momentum. Secondly, the production of particles in the intranuclear cascade and by evaporation processes must be correctly accounted for. Recently Ranft and Routti have described suitable empirical formulae which predict angular distributions in good agreement with available experimental data at all angles(115).

### 3. Accuracy of the Moyer Model

Use of the Moyer model with appropriate input data, and under fairly simple geometrical conditions, leads to estimates of radiation levels usually accurate to better than a factor of two. Figure 8 indicates the accuracy possible when experimental data are fitted to a Moyer-type equation. Calculated and measured neutron flux densities in the earth shield of the CPS are shown(116). Fluxes are plotted as a function of longitudinal distance from an internal target for five different depths in the shield. Flux densities were measured utilizing the  $^{27}\text{Al}(n, \alpha)^{24}\text{Na}$  reaction in aluminum. In this particular example, flux densities are predicted to about 20%, over a range of five orders of magnitude. Estimates of dose-equivalent rate follow from a knowledge of neutron flux density and spectrum.

For the calculation of shield thicknesses transverse to a proton beam, for uniform beam loss, the Moyer model takes a particularly simple form. Substituting for  $g(\theta)$  using Equation 12, and using experimental data from the CPS it may be shown that

$$\dot{\underline{H}} = \frac{0.11 \underline{L}}{(\underline{a} + \underline{d})} \int_0^{\pi} \exp(-2.3\theta) \exp\left(-\frac{\underline{d}}{\lambda} \operatorname{cosec} \theta\right) d\theta, \quad 14.$$

where  $\dot{\underline{H}}$  is measured in mrem/h,  
 $\underline{L}$  is the beam loss in units of GeV/cm sec,  
 $\underline{a}$  is the accelerator tunnel radius in meters,  
 $\underline{d}$  is the shield thickness in meters, and  
 $\lambda$  is the attenuation length.

Integrals of the form appearing in Equation 14 have been tabulated in the region of physical interest by Routti and Thomas(117).

Phenomenological models permit simple, rapid, and fairly accurate shield estimates. Furthermore, they provide a valuable physical insight into the problems of shielding. Such models are, however, necessarily limited by operational experience.

#### B. Monte Carlo Calculations

One of the most important advances in the study of accelerator radiation environments over the past ten years has been the development of Monte Carlo techniques to calculate electromagnetic and hadronic cascade phenomena. These calculations have recently been reviewed by Ranft(104), and space does not permit a complete discussion here. Accurate and reliable calculations of radiation phenomena at accelerators have required development of an understanding not only of the interaction of primary particles with internal targets and machine components, but also of particle production resulting from primary particle interaction, the transport of these primary and secondary particles together with

their interaction products through matter and, finally, the conversion from the calculation of particles transported to observable phenomena. Ranft has reported good agreement with experimental data in such diverse areas as induced radioactivity, radiation doses, radiation heating, and shielding.

A good example of the agreement between theoretical and experimental data is the recent calculation of the neutron spectrum in the earth's atmosphere by Armstrong et al (118). These workers used a Monte Carlo code to compute the production of protons, charged pions, and neutrons by the incident galactic protons, and the subsequent transport of these particles down to energies of 12 MeV. The production of neutrons of energy  $\leq 12$  MeV as calculated by the Monte Carlo code, was used as input to a discrete-ordinates code to obtain the low-energy neutron spectrum. Figure 9 shows the results of these calculations and an absolute comparison with the experimental data of Hess et al (38) at atmospheric depths of 200 and 1033 g/cm<sup>2</sup>. The calculated and measured spectra differ somewhat at lower energies but are in good agreement at high energies. The increasing number of such examples of good agreement between calculated and experimental data is extremely encouraging.

## 5. INDUCED RADIOACTIVITY

The development and transport of the electromagnetic and hadronic cascades (sections 3 and 4) also result in the production of radioactivity in accelerators and their surroundings. Accelerator shielding and accelerator components such as targets, vacuum chamber, magnets and rf cavities, cooling water or ground water close to the accelerator buildings, and air in the accelerator room may all become radioactive to some degree.

Barbier(119) has summarized the mechanism for the production of radioactivity at high-energy accelerators. In principle, all the nuclides which have atomic mass and atomic number equal to, or less than, the sum of the numbers of the target plus projectile nuclei can be produced. Many of the radionuclides that can be produced have half-lives so short that they need not be considered in protection problems.

### A. Radioactivity of Accelerator Components and Other Solids

The number of radionuclides which might be produced is potentially very large. Fortunately the materials used in accelerator construction are limited in number, the most important being iron, several stainless steels, copper, aluminum, aluminum alloys, and several plastics. Charalambus and Rindi(120) have reported a table of all the main radionuclides that can be produced at a typical proton accelerator. They considered only radionuclides with a half-life longer than one hour and show that about 70% of them are  $\gamma$ -emitters. However, even shorter half-lives may be of concern for protection purposes if they are produced in large quantities.

Table 4 summarizes the radionuclides commonly identified in materials used in accelerators; those with half-lives of less than 10 minutes are excluded. Most of the radionuclides listed are produced by simple nuclear reactions such as (n, xn), (p, xn), (p, pn) etc., but some result from spallation, fragmentation, or capture reactions.

Several measured cross sections for high-energy reaction have been reported by Bruninx(121-123). Rudstam(124) has proposed a very useful empirical formula for their calculation, while Bertini(125) has reported intranuclear cascade calculations of these cross sections.

Because the number of radionuclides produced in accelerator components is large and accelerator operation often variable, the production and decay of gross radioactivity is a complex function of time. Notwithstanding, for radiation protection purposes it may be necessary to have some estimate of the dose rate, and its variation with time.

The decay of dose rate near the 600-MeV CERN synchrocyclotron has been reported by Baarli(126) and Rindi(127). Reliable experimental data of this type are few because of the difficulty of obtaining them at most accelerators. During periods of accelerator shutdown, gross changes in the remnant radiation field may result from structural changes in the accelerator and its shielding. What data are available, however, show that beginning a few minutes after the shutdown, the dose rate decays by about a factor of two in the first two hours and by about another factor of two within the next 50 hours. This is in agreement with measurements at all the accelerators at the Lawrence Berkeley Laboratory(128), and elsewhere(129). Indeed it seems confirmed by general experience that the gross features of the decay of induced activity near accelerators

that have been in operation for several years, are nearly independent of the type of particles accelerated and their maximum energy.

Sullivan and Overton(130) have shown that the dose-rate decay may be approximated by an equation of the form

$$\underline{D}(t) = \underline{B} \phi \ln \left( \frac{T+t}{t} \right) \quad 15.$$

where  $\underline{D}(t)$  is the dose rate at time  $t$  after irradiation ceases,  $\phi$  is the flux density of high-energy primary particles,  $T$  is the irradiation time and  $\underline{B}$  is a parameter which depends on several variables but is a constant for any given set of irradiation, target and geometrical conditions. Equation 15 is in good qualitative agreement with the form of the build-up and decay of dose rates observed in an accelerator environment, and in a recent paper Sullivan(131) has reported values of  $\underline{B}$  for heavy materials that give reasonably good absolute agreement with observation. More accurate calculations require detailed Monte Carlo techniques of the type used in shielding calculations. (See section 4.) Armstrong et al (132, 133) have calculated the dose rate resulting from the irradiation of steel by 200-MeV, 3-GeV, and 200-GeV protons. For long irradiation times they find that  $^{52m}\text{Mn}$ (21 min),  $^{56}\text{Mn}$ (2.6 h),  $^{52}\text{Mn}$ (5.6d),  $^{48}\text{V}$ (16 d),  $^{51}\text{Cr}$ (27.8 d), and  $^{54}\text{Mn}$ (280 d) are the dominant radionuclides (Figure 10). These calculations are supported by recent observations at the 76-GeV proton synchrotron in Serpukhov(134).

At electron accelerators, too, only few nuclides are dominant. For example, Saxon(135) reports that at the 4-GeV electron synchrotron NINA,  $^{56}\text{Mn}$ ,  $^{52}\text{Mn}$ , and  $^{48}\text{V}$  are dominant in steel. Similar results have been reported by Wyckoff(136) from exposure to the 100-MeV

bremstrahlung beam of the NBS linac. De Staebler(137) has estimated the gross production of radioactivity by a high-energy electron accelerator as some 34 Ci at saturation per kW of beam power.

#### B. Radioactivity of Air

Radioactive gases are produced by the interaction of primary and secondary particles with the nitrogen, oxygen, argon, and carbon nuclei of air circulating in the accelerator vaults. In Table 5 we show the radionuclides which have been found in the air at different accelerators. Radionuclides with half-lives less than one minute are of no concern, decaying to negligible activities before personnel can enter the accelerator room or before the air can reach populated areas around the accelerator. Long-lived activities, on the other hand, may be discounted because of their low production rate. Such arguments, supported by the measurements cited in Table 5, suggest that at existing accelerators only four radionuclides need be considered:  $^{15}\text{O}$ ,  $^{13}\text{N}$ ,  $^{11}\text{C}$ , and  $^{41}\text{Ar}$ . A further increase in the energy or in the intensity of the accelerators however, could cause the production of amounts of  $^7\text{Be}$  and  $^3\text{H}$  which may be important.

Presently, the concentrations of radioactive gases measured in the accelerator room a few minutes after shutdown, may range between 10 and 30 times the MPC for continuous inhalation(139). However, the air is quickly mixed with inert air and the radioactivity decays rapidly so that the associated dose rate is negligible compared to that from the solid machine parts.

### C. Radioactivity of Water

Radioactivity induced in cooling water circuits of high-intensity accelerators is potentially of concern for the following reasons: high dose rates around pipes carrying this water, radioactive contamination resulting from spills, and disposal problems. Rose et al (146) reported that external radiation levels as high as 100 mrem/h were found at various regions close to the cooling system of the Harwell 150-MeV cyclotron when it was operated with an internal beam of about 1  $\mu$ A. Warren et al (147) have reported dose rates of between 0.5 and 4 mrem/h from cooling water circuits along the accelerator structure of the Stanford 20-GeV electron linear accelerator. Considerably higher levels are found from heat exchangers for high-power beam dumps—rates up to 120 mrem/h being observed.

Distenfeld(143) has concluded from measurements at the Brookhaven AGS that with a proton beam intensity of  $10^{13}$  protons/sec the external radiation hazard from induced activity in cooling water would be trivial. However, the dose rate from large volumes of water, such as heat exchangers or storage tanks, would be measurable during accelerator operation. Some rough experimental studies of the production of radionuclides in water from typical high-energy neutron spectra(148) have confirmed  $^{11}\text{C}$ ,  $^7\text{Be}$ , and  $^3\text{H}$  as the most important ones produced. The ratio of the specific activities of tritium and  $^7\text{Be}$  extrapolated at saturation in samples of water irradiated under several different conditions varied between 1.3 and 5.8. Disposal of irradiated water to streams would generally be controlled by the tritium content, since  $^7\text{Be}$  is strongly absorbed in the mixed bed resins used for

demineralizing the waters(149). Careful studies of the radioactivity produced in water irradiated by high-energy electrons (147) have identified  $^{15}\text{O}$ ,  $^{11}\text{C}$ , and  $^7\text{Be}$  as the most important radionuclides.

D. Environmental Impact of Radioactivity

The environmental impact of accelerators has been given some study over the past few years. Large accelerators are capable of producing many thousands of curies of radioactivity, a small fraction of which may be released to the environment. The transportation of these radionuclides, induced directly in ground water or leached from irradiated earth in the accelerator shield, has been studied around proton synchrotrons with energies up to several hundred GeV (150-153). These studies show that the inventory of long-lived radionuclides produced in earth shields of such accelerators is of the order of tens of curies, or less. Chemical sorption plays an extremely important role in preventing the migration of many of the nuclides. From these studies the levels of radioactivity likely to appear in ground water systems will be minimal and may not even be detectable.

## 6. CONCLUSIONS

We hope that in this brief review we have been able to indicate the advances in the qualitative and quantitative understanding of accelerator radiation problems that have been achieved in the past fifteen years. From almost complete ignorance of these problems we have reached the point where accurate estimates of shielding, induced radioactivity, radiation damage, and radiation levels are generally possible.

The increasing use of accelerators in industry and medicine necessitates the wider dissemination of our expanding knowledge of accelerator-produced radiation. There is a need to educate sufficient operating personnel as to the special problems of shielding and dosimetry at particle accelerators, if adequate safety standards are to be maintained. This need is especially important at accelerators used for radiation therapy, and is not fulfilled by specialized conferences open only to a limited audience. A number of recent monographs(4, 119, 154, 155) specifically discussing accelerator radiation problems will help alleviate this situation. In the United States a start has been made to provide more formal instruction through short training courses.

The radiation problems of very-high-energy accelerators (> 10 GeV) continue to be of rather specialized interest, but the systematic solution of these problems will be of general interest to other disciplines as well.

Despite the significant advances reported here, much remains to be done. The problems of personal dosimetry for high-energy neutrons

( $E > 20$  MeV) has, to date, been given little attention. Shield computations still need to be refined and this must be done by comparison with observation. Improvements are still needed in instrumentation for the measurement of fast neutrons "in the field." We suggest that the problems of induced radioactivity will need increasing study if the application of accelerators in industry is not to be inhibited. Radiation damage studies, too, are of increasing importance so that accelerators may be economically and efficiently designed.

### ACKNOWLEDGMENTS

It is a pleasure to thank H. Wade Patterson (Lawrence Berkeley Laboratory) and H. de Staebler (Stanford Linear Accelerator Center) for helpful advice in the preparation of this article. We are grateful to our colleagues of the several high-energy research centers for providing us with updated information on their researches.

Thanks are also due to LBL editor Mary Wildensten, to Mary Long of the Health Physics group, and to Carmen Hubbard for typing the manuscript.

This work was done under the auspices of the U. S. Atomic Energy Commission.

LITERATURE CITED

1. Rotblat, J. 1950. The Acceleration of Particles to High Energies, Sect. 1, pp 1-13. Institute of Physics, London
2. Livingston, M. S. 1952. Ann. Rev. Nucl. Sci. 1: 167
3. Patterson, H. W., Thomas, R. H. 1971. Part. Accel. 2: 77
4. Patterson, H. W., Thomas, R. H. 1973. Accelerator Health Physics. New York: Academic. In press
5. Ham, W. T. 1953. Am. Med. Assoc. Arch. Ophthalmol. 50: 618
6. Moyer, B. J. 1954. Radiation Res. 1: 10
7. Moyer, B. J. 1958. Ann. Rev. Nucl. Sci. 8: 327
8. De Staebler, H. 1962. Transverse Radiation Shielding for the Stanford Two-Mile Accelerator, USAEC Rep., SLAC 9
9. Los Alamos Scientific Laboratory 1964. A Proposal for a High Flux Meson Facility
10. Yale University Design Study Staff 1964. A Final Report on the Design of a Very High-Intensity Proton Linear Accelerator as a Meson Factory of 750 MeV. Yale Rep. Y-12
11. CERN Laboratory 1964. Report on the Design Study of a 300-GeV Proton Synchrotron. CERN Rep. 563 (2 vols.)
12. Lawrence Radiation Laboratory 1965. 200-BeV Accelerator Design Study Report. UCRL-16000 (2 vols.)
13. National Accelerator Laboratory 1968. Design Report (Revised version)
14. Awschalom, M. 1969. In Proc. Conf. Radiat. Prot. in Accelerator Environ. Rutherford Lab, England

15. Awschalom, M. 1971. Proc. Int. Congr. Radiat. Prot. Accelerator and Space Radiat. CERN Lab., Geneva, CERN 71-16:1050
16. Goebel, K. (ed.) 1971. Radiat. Problems Encountered in the Design of Multi-GeV Res. Facilities. CERN 71-12
17. Shaw, K. B., Stevenson, G. R., Thomas, R. H. 1969. Health Phys. 17: 459
18. Patterson, H. W., Routti, J. T., Thomas, R. H. 1971. Health Phys. 20: 517
19. Burlin, T. E., Wheatley, B. M. 1971. Phys. Med. Biol. 16: 47
20. Rindi, A., Thomas, R. H. 1972. Health Phys. 23: 715
21. Rosen, L. 1971. IEEE Trans. Nucl. Sci. NS-18: 29
22. Morgan, I. L. 1973. IEEE Trans. Nucl. Sci. In press
23. Burill, E. A. 1969. In Proc. Int. Conf. Accelerator Dosimetry, 2nd, Stanford, Calif. CONF-691101
24. Boom, M. L. M., Wiley, A. L. 1971. See Ref. 21, p 36
25. Raju, M. R., Richman, C. 1971. Current Topics in Radiat. Res. eds. M. Ebert and Howard, Amsterdam: North-Holland
26. Tobias, C. A., Lyman, J. T. Lawrence, J. H. 1971. Recent Advan. in Nucl. Med. Vol. 3, Chap. 6, ed. J. H. Lawrence, New York: Grune and Stratton, Inc.
27. See for instance, Schaefer, H. J. 1971. Science 173: 780
28. Holcomb, R. W. 1970. Science 167: 853
29. Rossi, H. H., Kellerer, A. M. 1972. Science 175: 200
30. ICRP 1972. Publication #18. Oxford: Pergamon
31. Patterson, H. W. 1957. Proc. Conf. Shielding High-Energy Accelerators, New York. USAEC Report TID-7545, p 3

32. Smith, A. R. 1958. LBL Rep. UCRL-8377
33. Smith, A. R. 1962. Proc. Premier Colloq. Int. sur la Prot. auprès des Grands Accélérateurs. Paris: Presses Universitaires de France
34. Patterson, H. W. 1965. Proc. Symp. Accelerator Radiat. and Dosimetry, 1st, BNL, Brookhaven. CONF-651109, p 3
35. Patterson, H. W., Hess, W. N., Moyer, B. J., Wallace, R. 1959. Health Phys. 2: 69
36. Tardy-Joubert, P. 1965. See Ref. 34, p 117
37. Tardy-Joubert, P. 1967. Progr. in Radiology, Vol. 2. Amsterdam: Excerpta Med. Found.
38. Hess, W. N., Patterson, H. W., Wallace, R. 1959. Phys. Rev. 116: 445
39. Puppi, G., Dallaporta, N. 1952. Progr. Cosmic Ray Phys. 1: 317
40. Baarli, J., Sullivan, A. H. 1965. Health Phys. 11: 353
41. Perry, D. R. 1966. Proc. Symp. Neutron Monitoring for Radiological Prot. Vienna: IAEA, p 355. See also Perry, D. R., Shaw, K. B. 1965 in Ref. 34, p 20
42. Komochkov, M. M. 1970. Eng. Compendium on Radiat. Shielding, Vol. 3: 171. New York: Springer-Verlag
43. Baarli, J. 1964. Private communication to Middlekoop, W. C., reported in CERN Intern. Rep. AR/INT/SG 64-6
44. Capone, T. et al 1965. CERN Intern. Rep. DI/HP/71
45. Baarli, J., Sullivan, A. H. 1965. See Ref. 34, p 103
46. Thomas, R. H. 1972. Proc. IAEA Symp. Neutron Dosimetry. Vienna: IAEA. In press

47. Lehman, R. L., Fekula, O. M. 1964. Nucleonics 22(11): 35
48. Rossi, B. 1954. High-Energy Particles. New York: Prentice-Hall
49. Remy, R. 1965. UCRL Rep. 16325
50. Omberg, R. P., Patterson, H. W. 1967. UCRL Rep. 17063
51. Patterson, H. W., Heckman, H. H., Routti, J. T. 1969. See Ref. 23, p 750
52. Gilbert, W. S. et al 1968. UCRL Rep. 17941
53. Sullivan, A. H. 1969. See Ref. 23, p 625
54. Smith, A. R. 1965. See Ref. 34, p 224
55. Smith, A. R. et al 1965. See Ref. 34, p 365
56. Bramblett, R. L., Ewing, R. I., Bonner, T. W. 1960. Nucl. Instrum. Methods 9: 1
57. Aleinkov, V. E., Gerat, V. P., Komochkov, M. M. 1972. See Ref. 46
58. Routti, J. T. 1969. See Ref. 23, p 494
59. Routti, J. T. 1969. Ph.D. Thesis. Univ. of California, Berkeley. UCRL Rep. 18514
60. Stevenson, G. R. 1972. See Ref. 46
61. Gabriel, T. A., Santoro, R. T. 1972. ORNL-TM-3945
62. Bathow, G., Freytag, E., Tesch, K. 1965. Nucl. Instrum. Methods 33: 261
63. Bathow, G., Freytag, E., Tesch, K. 1967. Nucl. Phys. 82: 669
64. Tesch, K. 1969. See Ref. 23, p 595
65. Busick, D. et al. 1969. See Ref. 23, p 782

66. Ladu, M. 1969. Progr. in Nucl. Energ. Series XII, Part 1, p 365.  
New York: Pergamon
67. Bathow, G., Freytag, E., Kajikawa, R., Köbberling, M. 1969.  
See Ref. 24, p 222
68. Farmer, B. J., Rainwater, W. J. 1968. Report 0-71100/8R-S.  
NASA Contract NAS 9-7565
69. Farmer, B. J., Johnson, J. H. Bagwell, R. G. 1972. Proc.  
Nat. Symp. Natural and Man-Made Radiat. in Space, p 142;  
NASA-TM-X-2440
70. Bathow, G., Freytag, E., Tesch, K. 1967. Nucl. Instrum.  
Methods 51: 56
71. De Staebler, H. 1965. See Ref. 34, p 429
72. Carter, T. G., Thomas, R. H. 1969. Stanford Univ. Intern.  
Rep. RHT/TN/69-11
73. Chakalian, V. M., Thomas, R. H. 1969. Stanford Univ. Intern.  
Rep. RHT/TN/69-11
74. Thomas, R. H. 1969. Stanford Univ. Intern. Rep. RHT/TN/69-18
75. Coleman, F. J., Thomas, D. C., Saxon, G. 1972. Daresbury  
Nucl. Phys. Lab. Rep. DNPL/P72
76. Pszona, S. et al 1972. INR Rep. 1415, Warsaw
77. Shaw, K. B., Thomas, R. H. 1967. Health Phys. 13: 1127
78. Cowan, F. P. 1962. See Ref. 33, p 143
79. Keefe, D. 1964. LBL Intern. Rep. UCID-10018
80. Keefe, D., Noble, C. M. 1968. Nucl. Instrum. Methods 64: 173
81. Bertel, E., de Séréville, B., Freytag, E., Wachsmuth, E. 1971.  
See Ref. 16, p 79

82. Theriot, D., Awschalom, M., Lee, K. 1971. See Ref. 16, p 641
83. Kang, Y. et al 1972. Part. Accel. 4: 31
84. Penfold, J., Stevenson, G. R. 1968. Rutherford Lab Report RP/PN/28
85. Hajnal, F. et al 1969. Nucl. Instrum. Methods 69: 245
86. Rindi, A. 1969. See Ref. 23, p 660
87. Lim, C. B. 1973. Ph.D. Thesis, Univ. of California, Berkeley; LBL-1719
88. Rindi, A., Thomas, R. H. 1971. Proc. Ann. Health Phys. Topical Symp., 6th, Richland, Washington. p 465
89. Boag, J. W. et al 1972. Brit. J. Radiol. 45: 314
90. Rossi, H. H. 1969. In Proc. Symp. Neutrons in Radiobiol., Oak Ridge, CONF-691106
91. Katz, R. 1971. Proc. Biophysical Aspects of Radiat. Quality, 11. Vienna: IAEA
92. Katz, R., Sharma, S. C., Homayoonfar, M. 1972. Health Phys. 23: 740
93. ICRP 1969. ICRP Publication #14. Oxford: Pergamon
94. Patterson, H. W., Thomas, R. H. 1970. Proc. Berkeley Symp. Math. Statistics, and Probability, 6th, Vol. 6: 313. Berkeley: Univ. Calif. Press
95. RBE Committee 1963. Health Phys. 9: 357
96. Neary, G. J. 1963. Phys. Med. and Biol. 7: 419
97. ICRP 1970. ICRP Publication #15, Para. 13. Oxford: Pergamon
98. ICRP 1972. Publication #22 (in press)

99. Figerio, N. A., Coley, R. F., Branson, M. H. 1973. Phys. Med. Biol. 18: 53
100. See for example, Auxier, J. A., Snyder, W. S., Jones, T. D. 1968. Radiat. Dosimetry, eds. F. H. Attix, W. C. Roesch, Chap. 6. New York: Academic
101. See for example, Fuller, E. W., Eustace, R. C. 1971 in Ref. 15, p 344, or Armstrong, T. W., Bishop, B. L. 1971. ORNL-TM-3304
102. Patterson, H. W., Thomas, R. H. 1973. See Ref. 4, Chap. 2
103. Jaeger, T. 1960. Grundzeuge der Strahlenschutz. Berlin: Springer-Verlag
104. Ranft, J. 1972. Part. Accel. 3: 129
105. Moyer, B. J. 1961. UCRL Rep. 9769
106. Moyer, B. J. 1962. See Ref. 33, p 65
107. Keefe, D., Scolnick, M. 1966. LBL Intern. Rep. AS/EXPER/01
108. Schimmerling, W., Devlin, T. J., Johnson, W., Vosburgh, K. G., Mishke, R. F. 1973. Phys. Rev. 67: 248
109. Stevenson, G. R., Shaw, K. G., Hargreaves, D. M., Lister, L. P., Moth, D. A. 1969. Rutherford Lab. Rep. RHEL/M/48
110. Charalambus, S., Goebel, K., Nachtigall, D. 1967. CERN Lab. Rep. DI/HP/97
111. Awschalom, M., Schimmerling, W. 1969. Nuovo Cimento 64A: 871
112. Levine, G. S. et al 1972. Part. Accel. 3:91
113. Ranft, J. 1967. Nucl. Instrum. Methods 48: 133 and 261
114. Ranft, J., Borak, T. 1969. Nat. Accelerator Lab. Rep. NAL-FN-193

115. Ranft, J., Routti, J. T. 1972. Part. Accel. 4: 101
116. Gilbert, W. S. 1967. Proc. Int. Conf. High Energ. Accel., 6th, Cambridge, Mass. p 221
117. Routti, J. T., Thomas, R. H. 1969. Nucl. Instrum. Methods 72: 157
118. Armstrong, T. W., Chandler, K. C., Barish, J. 1972. Neutron Phys. Div. Ann. Rep., ORNL-4800, p 63
119. Barbier, M. 1969. Induced Radioactivity. Amsterdam: North Holland
120. Charalambus, S., Rindi, A. 1967. Nucl. Instrum. Methods 56: 125
121. Bruninx, E. 1961. CERN Rep. 61-1
122. Bruninx, E. 1962. CERN Rep. 62-9
123. Bruninx, E. 1964. CERN Rep. 64-17
124. Rudstam, G. 1966. Zeit. Naturforsch. 21 A: 1027
125. Bertini, H. W. 1969. See Ref. 23, p 42
126. Baarli, J. 1962. See Ref. 33, p 123
127. Rindi, A. 1964. Colloq. Intern. sur la Dosimetrie des Irradiations dues a des Sources Externes, Paris. Vol. 2: 153
128. Boom, R. W., Toth, K. S., Zucker, A. 1961. ORNL Rep. 3158
129. Awschalom, M., Larsen, F. L., Sass, R. E. 1965. See Ref. 34, p 57
130. Sullivan, A. H., Overton, T. R. 1965. Health Phys. 11: 1101
131. Sullivan, A. H. 1972. Health Phys. 23: 253
132. Armstrong, T. W., Barish, J. 1969. ORNL Rep. TM-2383

133. Armstrong, T. W., Alsmiller, R. J. 1969. Nucl. Sci. Eng. 38: 53
134. Golovachik, V. T., Britvich, G. I., Lebedev, V. N. 1969. IFVE-69-76. Transl. ORNL-tr-2328
135. Saxon, G. 1969. DNPL Rep. P8. Daresbury, England
136. Wyckoff, J. 1967. IEEE Trans. Nucl. Sci. 14(3) 990
137. De Staebler, H. 1963. SLAC Rep. TN-63-92. Stanford, Calif.
138. Vialettes, H. 1969. See Ref. 23 p 121
139. Rindi, A., Charalambus, S. 1967. Nucl. Instrum. Methods 47: 227
140. Höfert, M. 1969. See Ref. 23, p 111
141. Awschalom, M., Larsen, F., Schimmerling, W. 1968. Health Phys. 14: 345; idem 1969. Nucl. Instrum. Methods 75: 93
142. Shaw, K. B., Thomas, R. H. 1967. Health Phys. 13: 1127
143. Brookhaven Nat. Lab. 1964. BNL Rep. 7956, p 225
144. George, A. C., Breslin, A. T., Haskins, T. W., Ryan, R. M. 1965. See Ref. 34, p 513
145. Ladu, M., Pelliccioni, M., Roccella, M. 1967. Giorn. Fis. San. Minerva Fis. Nucl. 11(2): 112
146. Rose, B. et al 1958. AERE NP/R-2768. Harwell, England
147. Warren, G. J., Busick, D. D., McCall, R. C. 1969. See Ref. 23, p 99
148. Stapleton, G. B., Thomas, R. H. 1967. Rutherford Lab. Rep. RHEL RP/PN/45
149. Busick, D. D., Warren, G. T. 1969. See Ref. 23, p 139
150. Stapleton, G. B., Thomas, R. H. 1972. Health Phys. 23: 689

151. Thomas, R. H. 1970. Proc. Symp. Health Phys. Aspects of Nucl. Facility Siting, Idaho Falls, Idaho. p 93
152. Stapleton, G. B., Thomas, R. H. 1973. Water Research.  
In press
153. Borak, T. D. et al 1972. Health Phys. 23: 679
154. Zaitsev, L. N., Komochkov, M. N., Sychev, B. S. 1971.  
Fundamentals of Shielding Around Accelerators. Moscow:  
Atomizdat. (In Russian)
155. Freytag, E. 1972. Strahlenschutz an hochenergiebeschleunigern.  
Karlsruhe: G. Braun. (In German)

Table 1. Composition of radiation fields above thick shields at the CPS

Radiation component	Percentage of dose equivalent	
	Above concrete shield bridge <sup>a</sup>	Above target through earth shield <sup>b</sup>
Thermal neutrons	11-12	< 1-3
Fast neutrons (0.1 MeV < E < 20 MeV)	50-70	10-37
High-energy particles (E > 20 MeV)	2-25	52-89
$\gamma$ rays and ionization from charged particles	2-19	1-13

<sup>a</sup> Ref. 43

<sup>b</sup> Ref. 44, 45

Table 2. Effective conversion factors for neutron spectra

Spectrum	Effective neutron conversion factors	
	$\left( \frac{\text{n/cm}^2 \text{ sec}}{\text{mrem/h}} \right)$	
	Gilbert et al (52)	Shaw et al (17)
Cosmic ray	12.1	14.1
Bevatron	8.8	11.9
CERN synchrotron bridge	7.3	12.1
CERN ringtop	4.3	5.1
1/E	4.7	6.4

Table 3. Values of relaxation parameters

Detector	Assumed reaction threshold	Relaxation parameter b, radians <sup>-1</sup>				
		7 GeV data <sup>a</sup>			3 GeV data <sup>b</sup>	
		'W'	Cu	Al	Pb	Fe
HPD <sup>c</sup> & TLD		1.65±0.1	1.36±0.05	1.25±0.05		
<sup>32</sup> S - <sup>32</sup> P	3.0±0.5 MeV	0.29±0.03	0.39±0.04	0.50±0.06	0.23±0.07	0.30±0.08
<sup>27</sup> Al - <sup>24</sup> Na	6.0±0.5 MeV	0.51±0.02	0.65±0.04	0.71±0.04		
<sup>19</sup> F - <sup>18</sup> F	11±1 MeV	0.73±0.05	0.90±0.05	1.05±0.07		
<sup>12</sup> C - <sup>11</sup> C	22±3 MeV	1.28±0.05	1.34±0.03	1.32±0.05	1.10±0.12	1.35±0.16
<sup>12</sup> C - <sup>7</sup> Be	35±5 MeV	1.6 ±0.1	1.7 ±0.1	1.4 ±0.2		
<sup>27</sup> Al - <sup>18</sup> F	35±5 MeV	1.6 ±0.1	1.7 ±0.1	1.4 ±0.2	0.84±0.14	1.07±0.13
Au fission	90±10 MeV	2.1 ±0.3	2.1 ±0.3	2.1 ±0.3		

<sup>a</sup>Ref. 112

<sup>b</sup>Ref. 111

<sup>c</sup>Hydrogen pressure dosimeter

Table 4. Radionuclides commonly identified in solid materials irradiated around accelerators

Irradiated material	Radionuclides
Plastics, oils	$^7\text{Be}$ , $^{11}\text{C}$
Concrete, aluminum	As above, plus $^{22}\text{Na}$ , $^{24}\text{Na}$ , $^{32}\text{P}$ , $^{42}\text{K}$ , $^{95}\text{Ca}$
Iron, steel	As above, plus $^{44}\text{Sc}$ , $^{44\text{m}}\text{Sc}$ , $^{46}\text{Sc}$ , $^{47}\text{Sc}$ , $^{48}\text{V}$ , $^{51}\text{Cr}$ , $^{52}\text{Mn}$ , $^{52\text{m}}\text{Mn}$ , $^{54}\text{Mn}$ , $^{56}\text{Mn}$ , $^{57}\text{Co}$ , $^{58}\text{Co}$ , $^{60}\text{Co}$ , $^{57}\text{Ni}$ , $^{55}\text{Fe}$ , $^{59}\text{Fe}$
Copper	As above, plus $^{65}\text{Ni}$ , $^{61}\text{Cu}$ , $^{64}\text{Cu}$ , $^{63}\text{Zn}$ , $^{65}\text{Zn}$

Table 5. Radionuclides identified in the air of different accelerators

Radionuclide	Where identified	Explanation of previous symbol and reference
$^7\text{Be}$	A	A = Saclay 560-MeV electron linac (138)
$^{11}\text{C}$	A, B, C, D, E, F	
$^{13}\text{N}$	A, B, C, D, E, F, G, H	B = CERN 600-MeV proton synchrotron (139)
$^{14}\text{O}$	D	C = CERN 28-GeV proton synchrotron (140)
$^{15}\text{O}$	A, C, D, E, G, H	
$^{16}\text{N}$	E	D = PPA 3-GeV proton synchrotron (141)
$^{24}\text{Na}$	A, D	
$^{37}\text{S}$	D	E = RHEL 7-GeV proton synchrotron (142)
$^{38}\text{Cl}$	A, H	
$^{39}\text{Cl}$	A	F = BNL 30-GeV proton synchrotron (143)
$^{41}\text{A}$	A, B, C, D, F	
$^{34\text{m}}\text{Cl}$	D	G = RPI 50-MeV electron linac(144) H = Frascati 300-MeV electron linac (145)

### FIGURE CAPTIONS

Figure 1. Some typical high-energy neutron spectra (see Ref. 17).

- a.  $1/E$  spectrum (for comparison).
- b. cosmic-ray spectrum.
- c. spectrum at concrete shielding bridge at CPS.
- d. spectrum on earth shield of CPS.
- e. spectrum outside Bevatron shielding.
- f. spectrum outside steel shielding of Nimrod external proton beam.

Figure 2. Quality factor as a function of linear energy transfer in water, interpolated from ICRP recommendations(98).

Figure 3. Conversion factors as a function of energy for different particles.

Figure 4. Schematic diagram of typical shielding geometry.

Figure 5. Relative flux-density distribution measurements along paths drawn at several angles to the point of incidence of the proton beam on a concrete shield. Measurements made with the  $^{27}\text{Al} \rightarrow ^{24}\text{Na}$  reaction. Incident proton energy 6 GeV(55).

Figure 6. Typical example of the ratio of detector response as a function of distance from the point of incidence to the proton beam on the shield. The figure demonstrates the existence of an equilibrium spectrum. The curve labeled "axial profile" was obtained in the beam direction; that labeled "lateral profile" was obtained at a depth of four feet into the

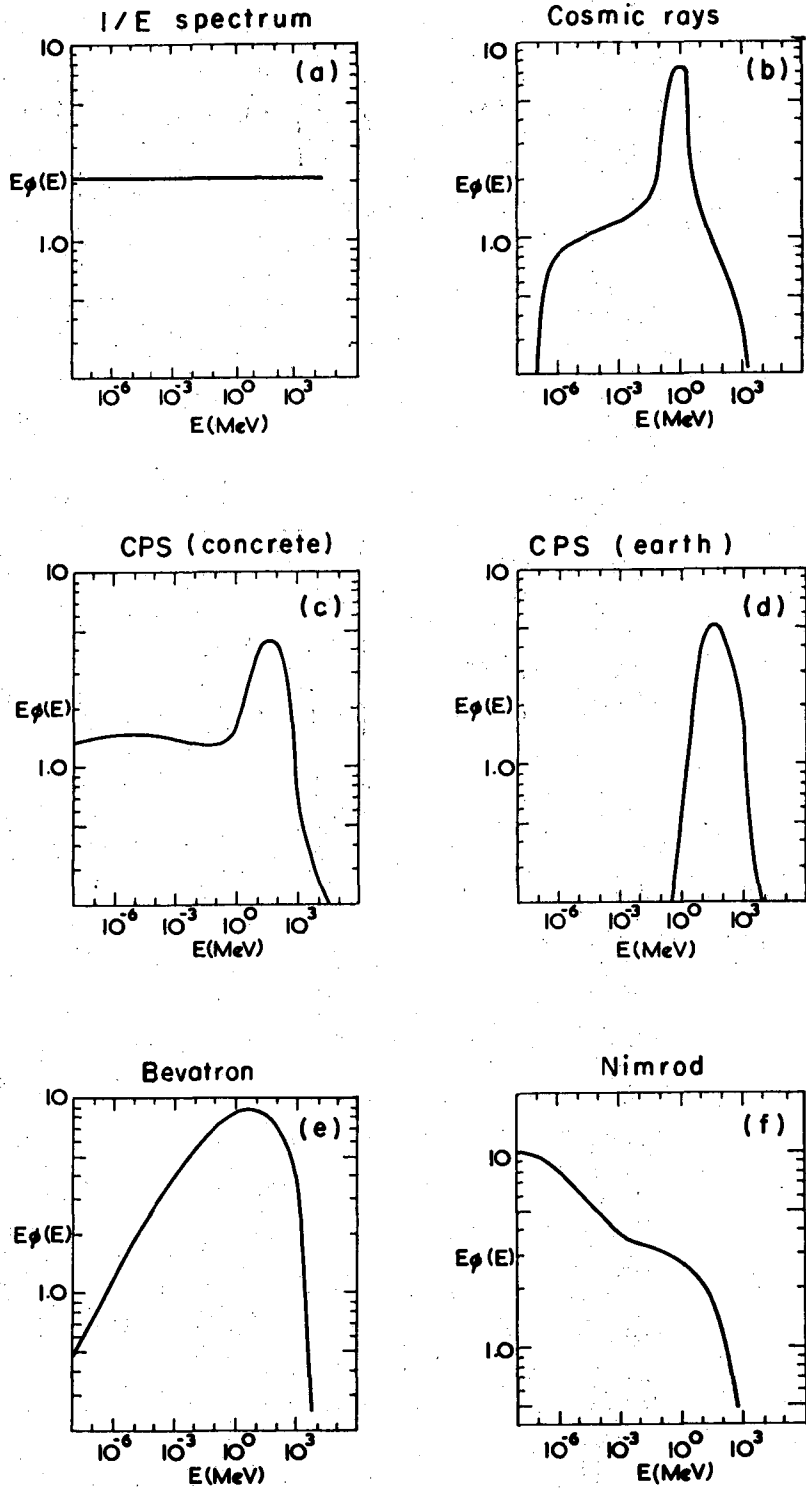
shield in a direction normal to the beam direction. Incident proton energy 6 GeV(55).

Figure 7. Angular relaxation parameter,  $b$ , as a function of reaction threshold energy (after Levine et al, 112).

Figure 8. Comparison of measured and calculated flux density as a function of position in the earth shield of the CPS. The abscissa gives the distance along the beam line measured from an arbitrary point. The 25-GeV proton beam interacted with a beryllium target at T(12.5 m from the origin). The ordinate shows the neutron flux density measured with an Al detector(116).

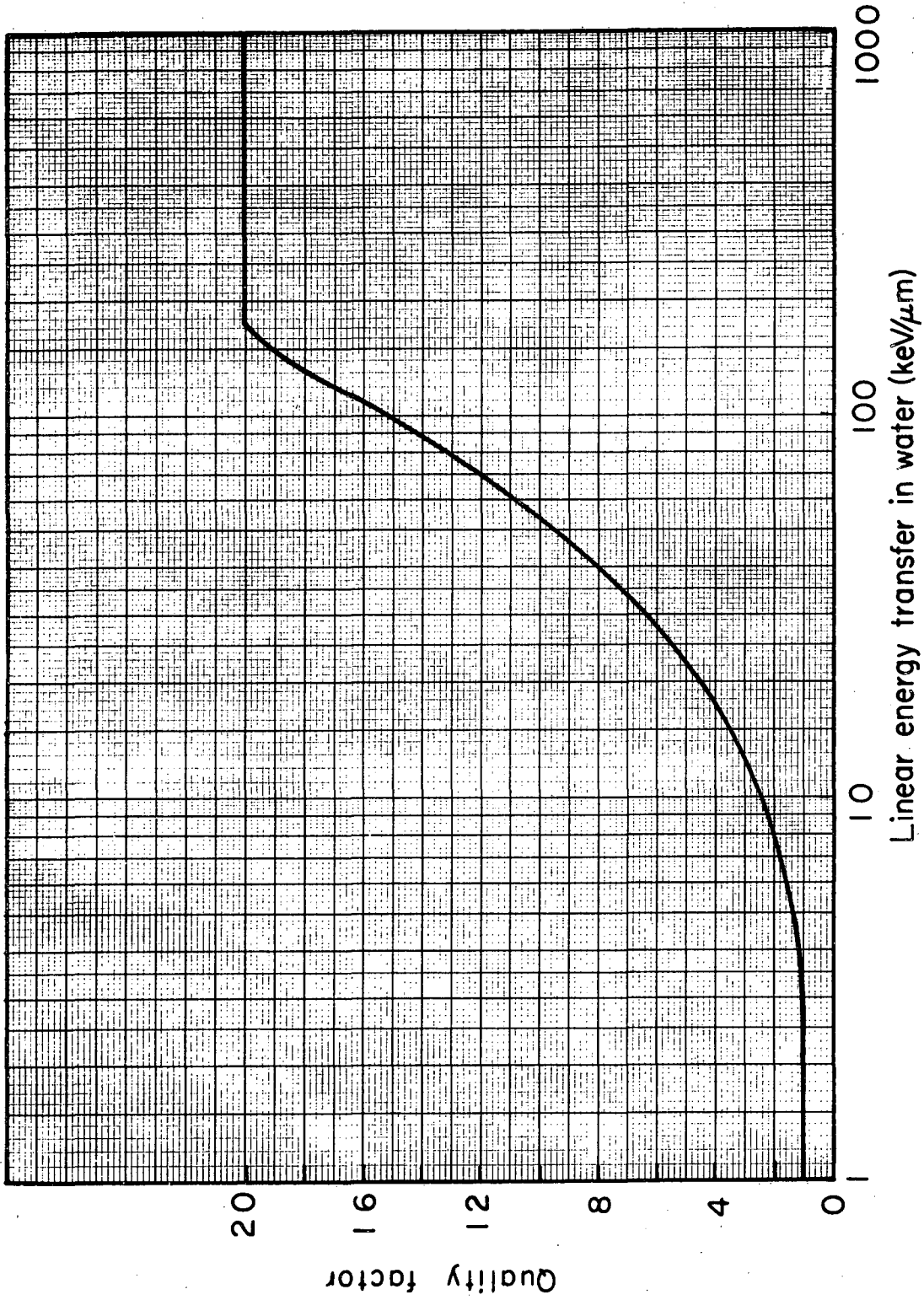
Figure 9. Histograms show calculated values of the cosmic-ray neutron spectra due to Armstrong et al(118), which are compared with the measurements of Hess et al(38) (solid line) at depth in the atmosphere of  $200 \text{ g/cm}^2$  and  $1033 \text{ g/cm}^2$  and are also compared with calculations of Lingenfelter-quoted by Armstrong et al (118)-at the top of the atmosphere (dotted lines). The calculations and measurements are made in the range of geomagnetic latitudes  $40-44^\circ$ .

Figure 10. Relative contribution to the photon dose rate due to six radionuclides at the surface of an iron cylinder (diameter  $80 \text{ g/cm}^2$ ) irradiated axially by 200-MeV and 3-GeV protons for an infinite time (from Armstrong and Barish, 132).



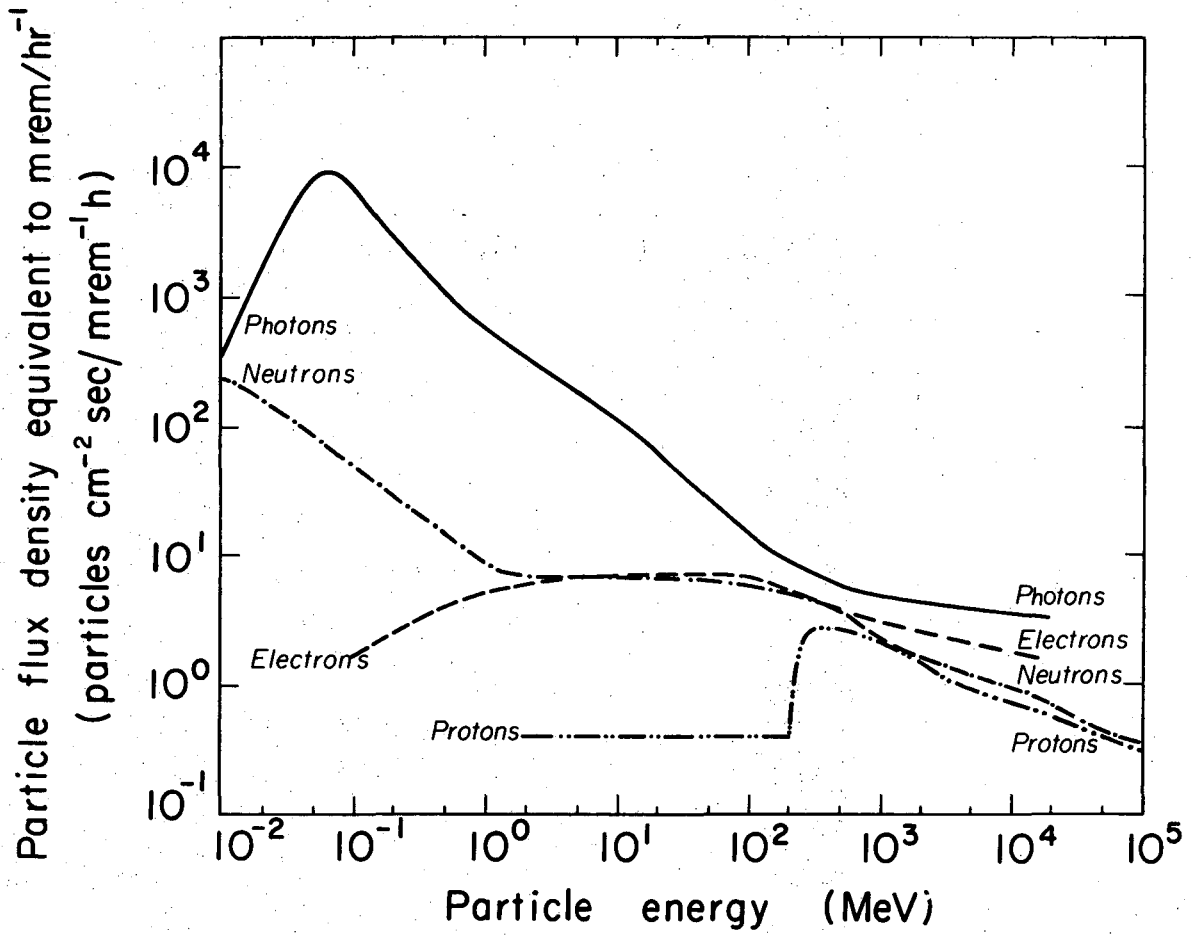
XBL733-2472

Fig. 1



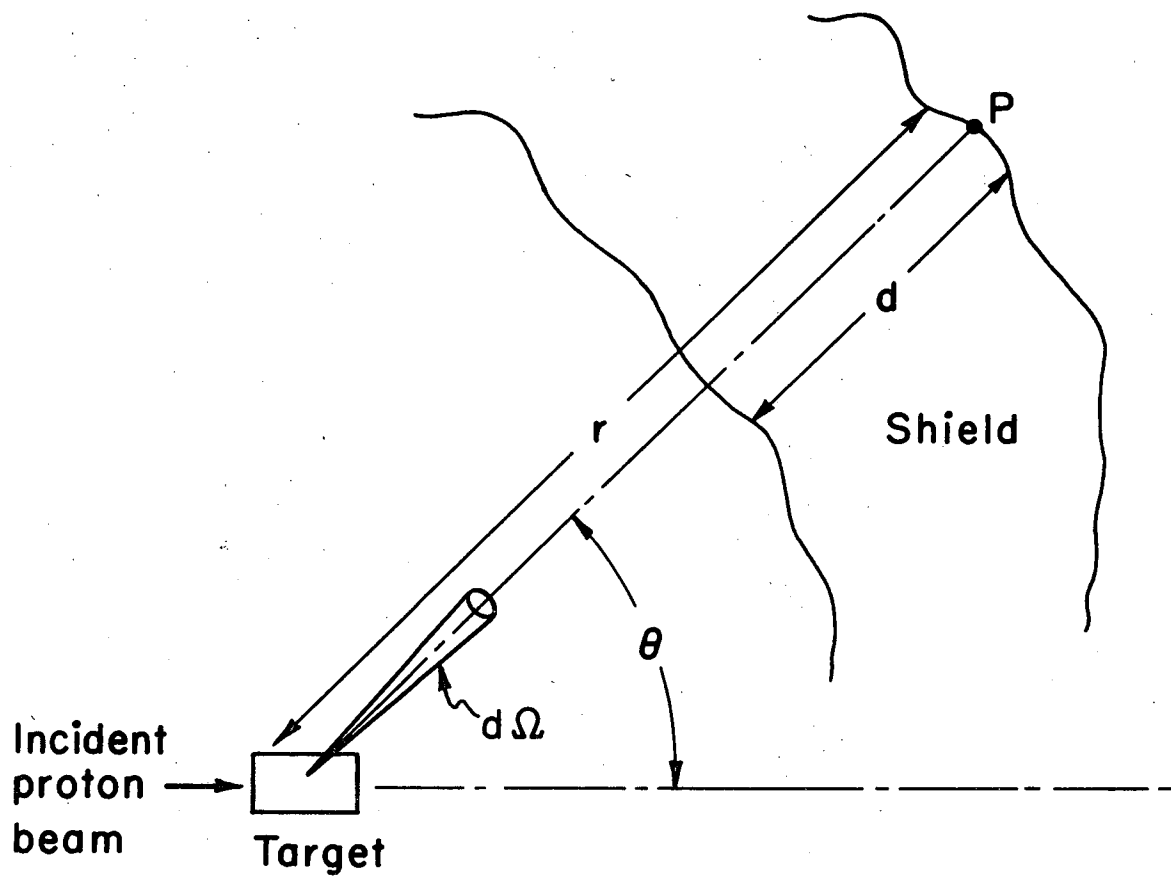
XBL733-2476

Fig. 2



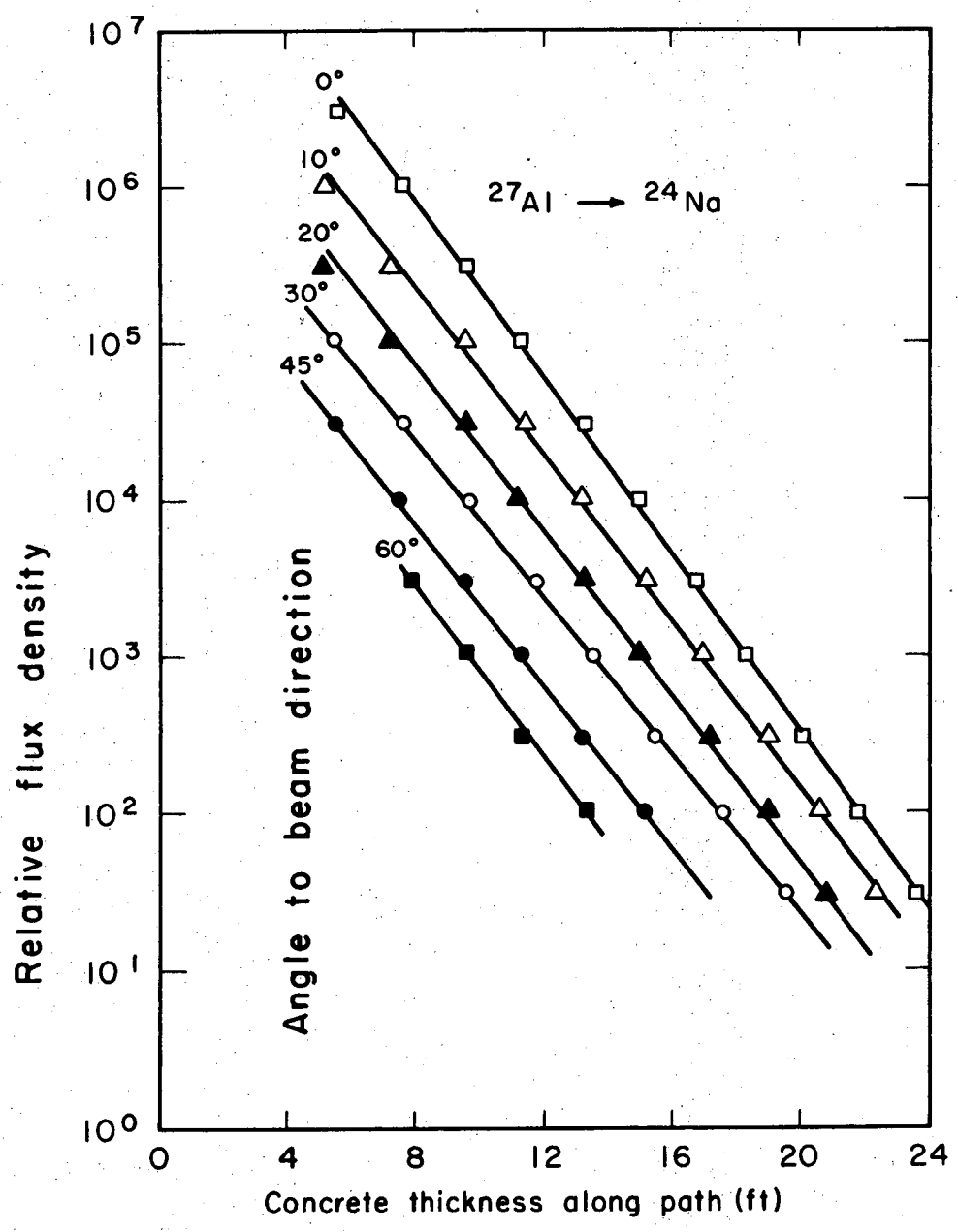
XBL733-2361

Fig. 3



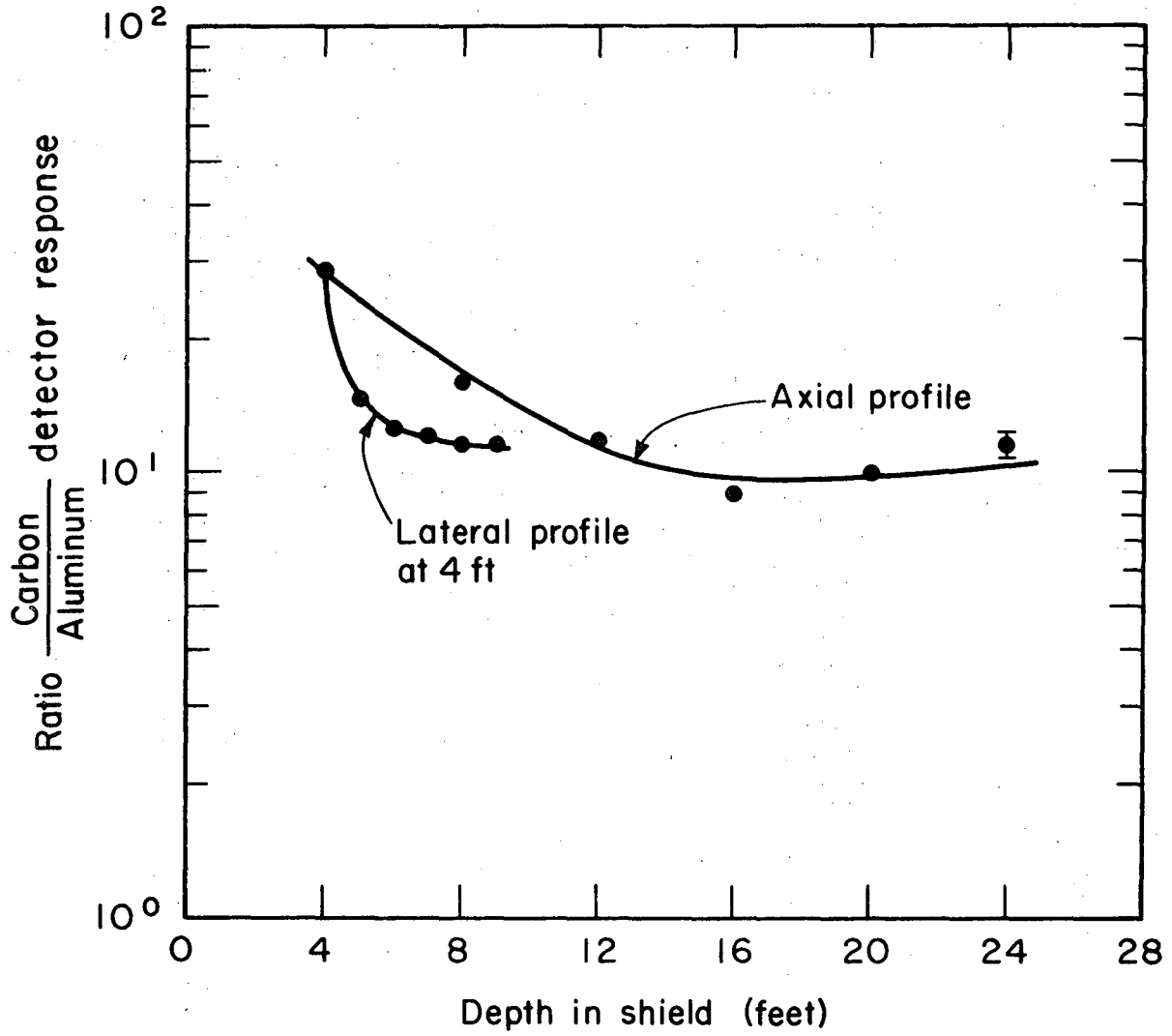
XBL 733-2478

Fig. 4



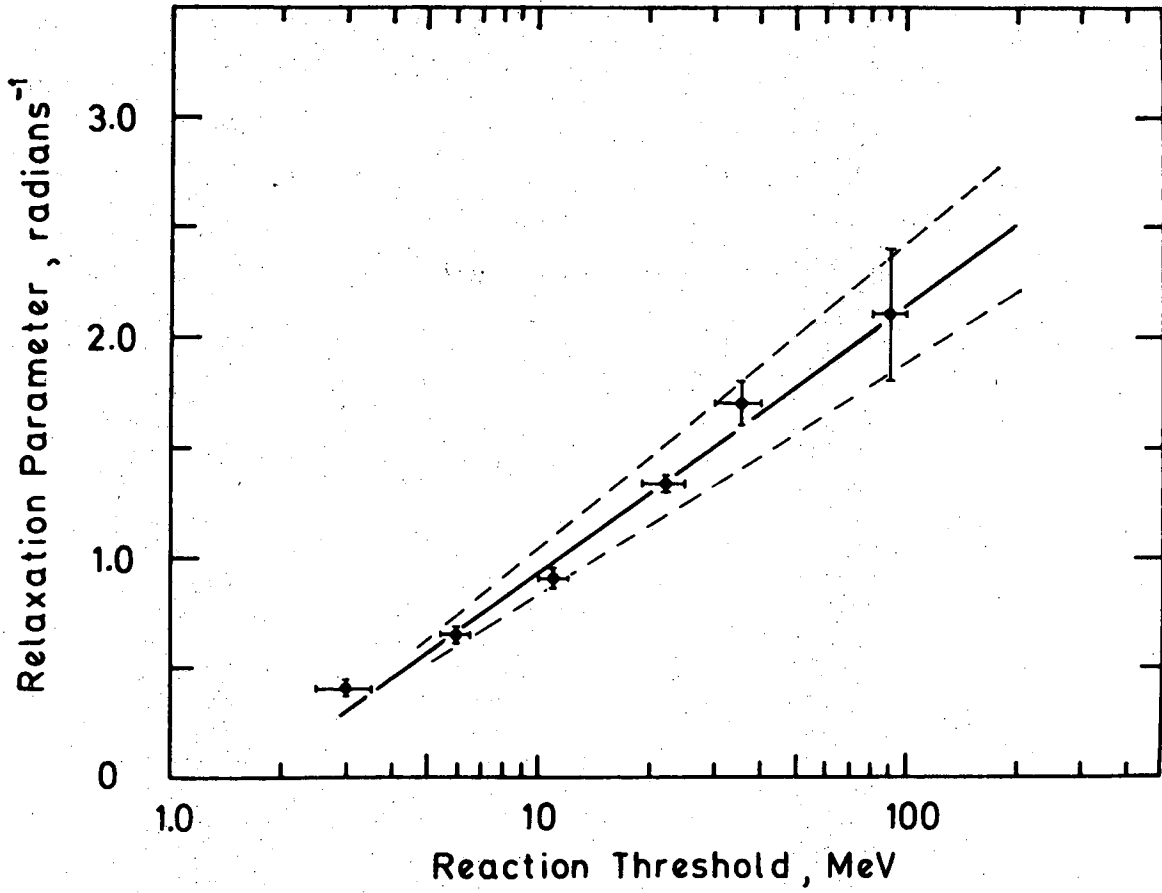
MUB-4051A

Fig. 5



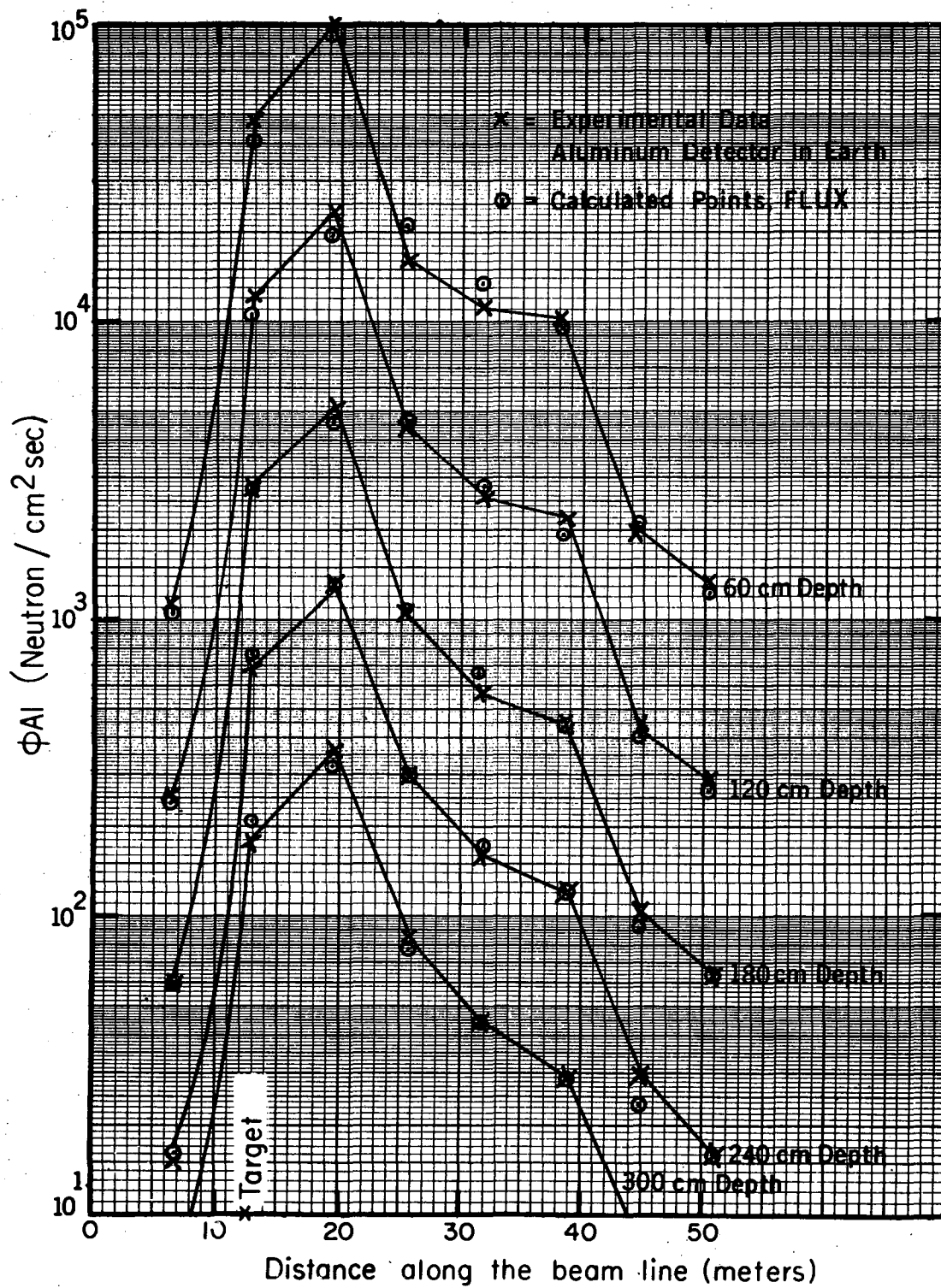
MUB-8448 A

Fig. 6



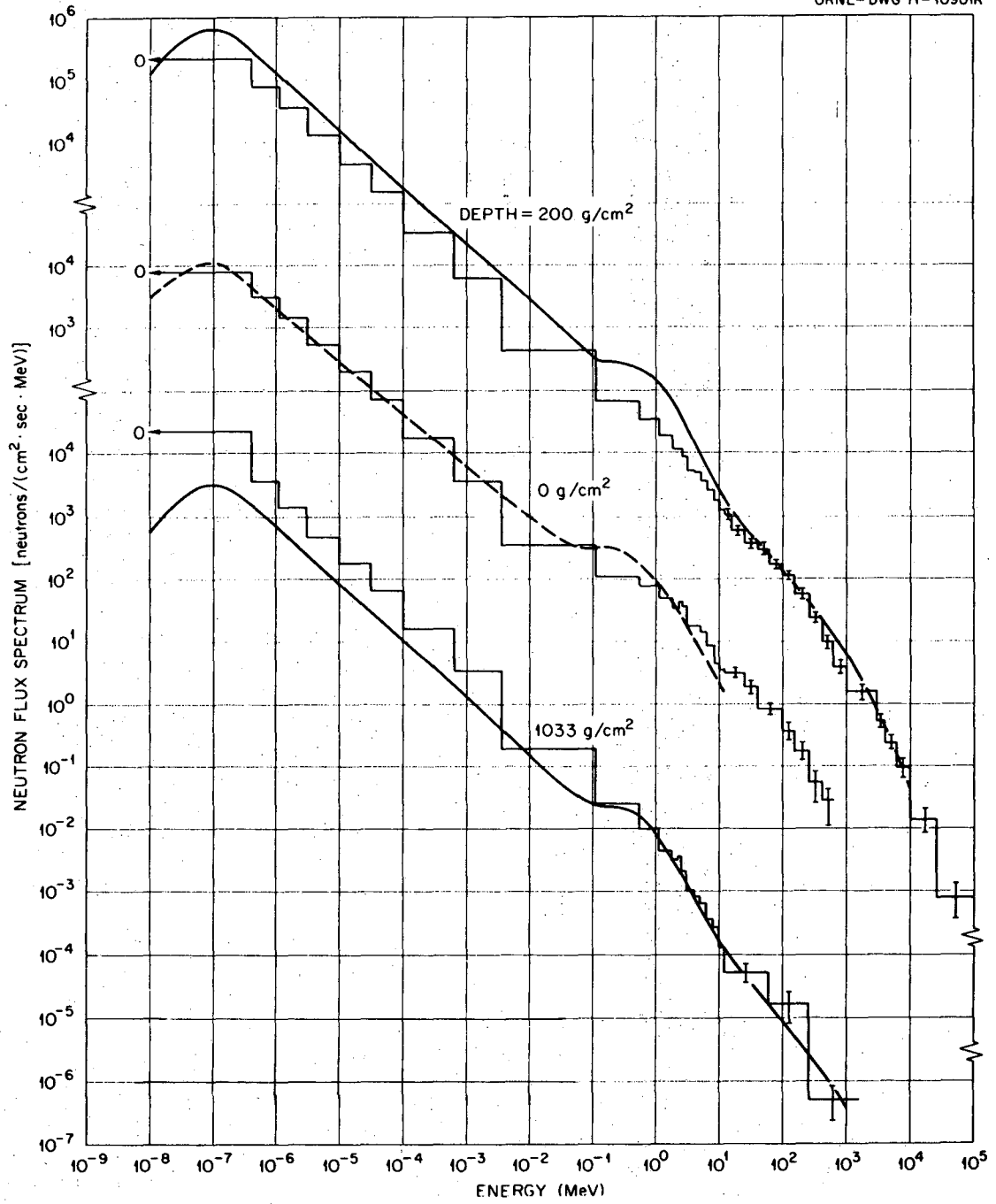
XBL 732-211

Fig. 7



XBL733-2477

Fig. 8



XBL 729-1939-A

Fig. 9

ORNL-DWG 68-14548R

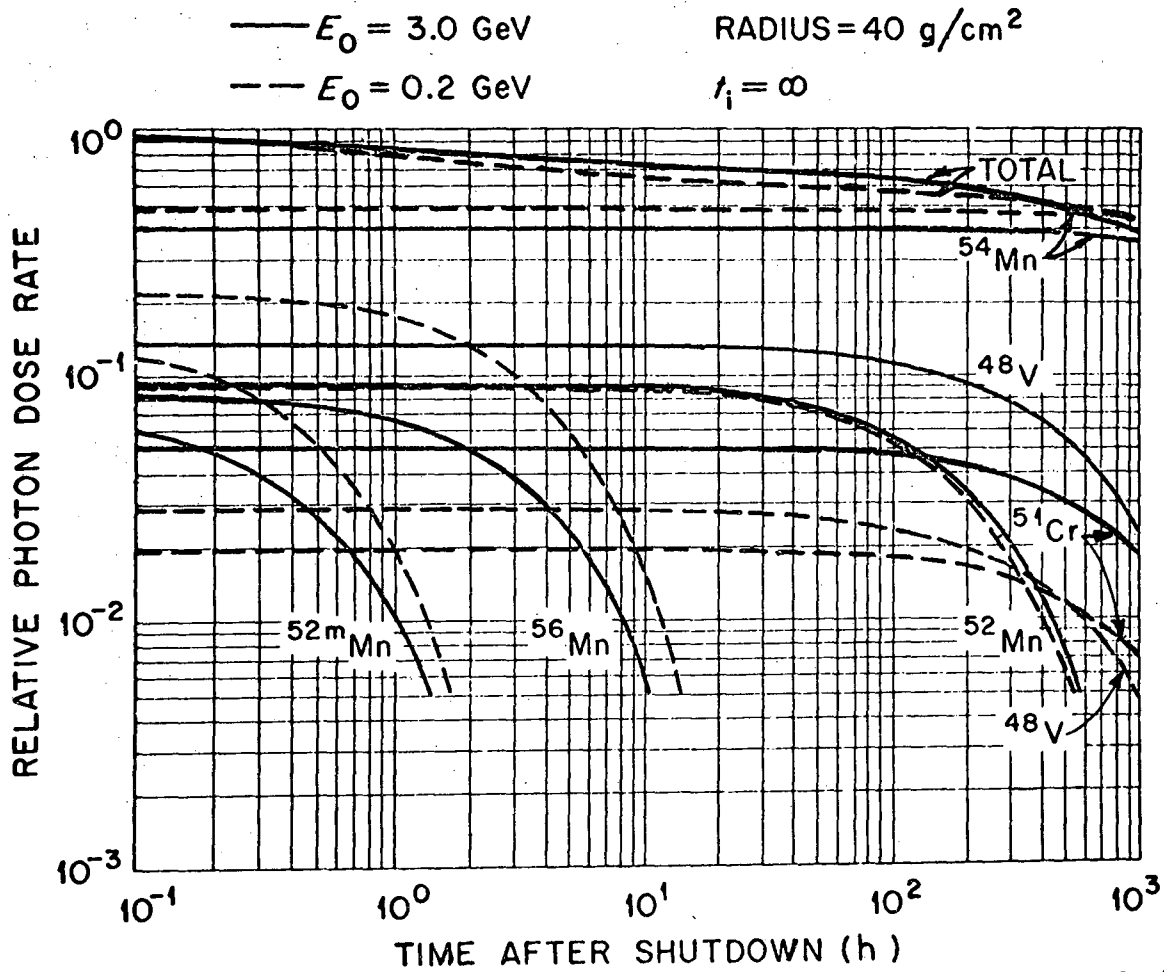


Fig. 10

LEGAL NOTICE

*This report was prepared as an account of work sponsored by the United States Government. Neither the United States nor the United States Atomic Energy Commission, nor any of their employees, nor any of their contractors, subcontractors, or their employees, makes any warranty, express or implied, or assumes any legal liability or responsibility for the accuracy, completeness or usefulness of any information, apparatus, product or process disclosed, or represents that its use would not infringe privately owned rights.*

TECHNICAL INFORMATION DIVISION  
LAWRENCE BERKELEY LABORATORY  
UNIVERSITY OF CALIFORNIA  
BERKELEY, CALIFORNIA 94720